IEEE Access
Multidisciplinary | Rapid Review | Open Access Journal

Received September 7, 2020, accepted October 5, 2020, date of publication October 7, 2020, date of current version October 19, 2020.

Digital Object Identifier 10.1109/ACCESS.2020.3029321

Design and Experimental Validation of the Temperature Control of a PEMFC Stack by Applying Multiobjective Optimization

SANTIAGO NAVARRO GIMÉNEZ, JUAN MANUEL HERRERO DURÁ, FRANCESC XAVIER BLASCO FERRAGUD, AND RAÚL SIMARRO FERNÁNDEZ
Instituto Universitario de Automática e Informática Industrial, Universitat Politècnica de València, 46022 Valencia, Spain

Corresponding author: Santiago Navarro Giménez (sannagi@etsii.upv.es)

This work was supported in part by the Spanish Ministry of Science, Innovation, and Universities under Grant RTI2018-096904-B-I00, and in part by the Generalitat Valenciana Regional Government under Project AICO/2019/055.

ABSTRACT The current environmental challenges require the implementation of environmentally friendly energy production systems. In this context, proton exchange membrane fuel cell stacks (PEMFC) represent, due to their high electrical efficiency and their low level of CO_2 emissions, a promising alternative technology. However, there are still many technical aspects that need to be improved before they become a commercial reality. One of them is the temperature control of the stack, since its electrical efficiency and its lifetime depend on the performance of this control. In this work, we design a multiloop PID control of the temperature of a PEMFC stack and validate it experimentally. The stack is the prime mover of a micro combined heat and power system (micro-CHP). For this task, we use a previously developed nonlinear model and apply a multiobjective optimization methodology. To assess its performance, the PID control is compared to a second PID control designed with a linearized model. The results show, on the one hand, the importance of having a nonlinear model valid in a wide operation range for the correct design of the temperature control of a PEMFC stack and, on the other hand, the advantages of applying a multiobjective optimization methodology to this problem.

INDEX TERMS PEMFC, temperature control, electrical efficiency, multiobjective optimization, PID control.

I. INTRODUCTION

The current environmental problems (global warming, air pollution, depletion of fossil fuel reserves) signal the need to turn towards sustainable energy production systems. PEMFC stacks, due to their high electrical efficiency and their low level of CO_2 emissions, are an efficient and clean alternative for many power generation applications: micro-CHP, back-up systems, hybrid electric vehicles (HEV), hybrid renewable energy systems (HRES) [1]–[3].

In these applications, the temperature control of the stack is crucial for its optimal operation. This is due to the fact that the electrical efficiency and the lifetime of the stack depend on the performance of this control, i.e. a good temperature control increases the electrical efficiency of the stack and its lifetime. In effect, at high temperatures the electrical efficiency of the stack increases (due to the increased conductivity of the membranes). However, if a certain threshold temperature is exceeded, the electrical efficiency begins to drop due to the dehydration of the membranes. This dehydration, in addition, increases the deterioration of the stack and, consequently, reduces its lifetime. Therefore, there is an optimum operating temperature at which the electrical efficiency of the stack is maximum and its deterioration is minimal [4]–[13].

In order to cool the stack and keep its temperature at its optimum value, a cooling system is used. This system is subject to the influence of various disturbances that can move the stack away from its optimum operating point. Among them, the most relevant is the electric current demand, because it causes most of the undesirable transients in the stack temperature (variations with respect to its optimum operating temperature). A good temperature control should be able to

The associate editor coordinating the review of this manuscript and approving it for publication was Huaqing Li.

react to the electric current demand so that the span and amplitude of these transients are as small as possible.

But maintaining the stack temperature at its optimum value is not the only objective of the temperature control. This should also maintain a uniform temperature gradient in the stack to avoid thermal stress [4], [36]. Furthermore, the temperature control should take into account the parasitic power consumption of the actuators, which affects the overall electrical efficiency of the system [1], [6], [9], [14]. Therefore, in the design of the temperature control of a PEMFC stack there is not a single objective, but several [15].

In order to design a good temperature control, it is necessary to have a model of the stack cooling system, a control-oriented model experimentally validated. This model should be dynamic, nonlinear and valid within a wide operating range, since the stack is a strongly nonlinear process. In the literature, there are many theoretical models, but few are dynamic and experimentally validated [5], [16], [17].

As a consequence of the lack of suitable models, many of the temperature controls that have been presented to date are based on linear models which are valid only at an operating point. For this reason, the validity range of these controllers is local [5]. Moreover, in the area of temperature control design we find the same situation as in modeling: very few of these temperature controllers have been experimentally validated.

For example, Ahn and Choe [9] designed a state-space control based on a control-oriented model and compared it to a classic PID control. They took into account the parasitic power consumption of the actuator, but the controller was not experimentally validated. Han *et al.* [14] designed a state-space controller using a linearized model. They took into account the parasitic power consumption of the actuators (radiator and pump), but they did not validate experimentally. In [18], Chen *et al.* developed an adaptive thermal control based on a nonlinear model and they also compared it with a classic PID control. However, they did not take into account control efforts nor verified experimentally their results. Rojas *et al.* [19] designed a model predictive control (MPC) based on a linearized model. No experimental validation. Similarly, Zhao and Pistikopoulos [20] designed a parametric model predictive control (pMPC) using a linearized model, but they did not carry out its experimental validation.

In the five articles introduced in the previous paragraph, the researchers worked with PEMFC stacks. An analogous situation is found in studies carried out with SOFC (solid oxide fuel cell) stacks. For example, Cao and Li [31] designed a multivariable robust proportional-integral derivative (PID) control system with a multiloop feedforward/feedback control structure for temperature control of a SOFC stack. In this work control efforts were not taken into account (parasitic power consumption of the actuators was, therefore, not considered) and the controller designed was tested only in simulation, without experimental validation. Huo *et al.* [32] developed a temperature controller for a SOFC stack, a variable structure controller (VSC). Control design was performed using a linearized model valid around an operating point. Control efforts were not taken into account and the controller designed was not experimentally validated. In [33], Mueller *et al.* designed an H-infinity output feedback controller for load perturbations (also for a SOFC stack). Here, again, control design was performed using a linearized model, control efforts were not considered, and experimental validation of the designed controller was not carried out.

All of these studies represent significant contributions to the area of fuel cell temperature control. However, as can be inferred from the analysis carried out in the two previous paragraphs, in general the works available to date in the area of fuel cell temperature control (both with PEMFC and SOFC stacks) have three shortcomings: 1) control designs are based on linearized models, so the validity range of these controllers is local (given the strong non-linearities existing in the real systems), 2) control efforts are usually not taken into account in the design, thus ignoring the global electrical efficiency of the system, and 3) the controllers designed are almost never experimentally validated, so their performance is not guaranteed. In this article, we try to overcome these three shortcomings.

In this work, first, we design a multiloop PID temperature control of a water-cooled PEMFC stack. This stack is the prime mover of a real micro-CHP system located in our laboratory (Predictive Control and Heuristic Optimization Group, CPOH, `http://cpoh.upv.es`). The design of this control is based on a model of the stack cooling system which was developed in a previous article [17]. This model is a control-oriented model, dynamic, nonlinear, based on first principles and it was experimentally validated within a wide operating range.

For the adjustment of the control parameters we use a multiobjective optimization methodology. Thanks to it, it is possible to consider several control objectives simultaneously. In particular, in this design we take into account the stack temperature, its temperature gradient and the control efforts. This methodology also has the advantage that it provides the designer with more information about the problem, which leads to a better decision-making and to the choice of a controller with a better performance.

Multiobjective optimization methodology has been used by several authors for the design of SOFC-based power generation systems [26]– [30]. In these works, various design parameters are optimized by using economic, environmental and energy efficiency indicators. Special mention deserves [34], which, methodologically, is similar to our research. In this work, multiobjective optimization is applied to tune the controller parameters of a SOFC stack. The controlled variables are output voltage and fuel utilization. It is not, therefore, a temperature control. The control design is based on a linearized model and the study is carried out only in simulation.

Secondly, in order to demonstrate the goodness of the designed control and the appropriateness of the methodology employed, we perform a comparative analysis in simulation. The performance of the control designed using the nonlinear

model is compared to that of a second control designed using a linearized model valid around an operating point.

Third and lastly, the theoretical results obtained in simulation are experimentally verified in the real micro-CHP system.

The experimental data corroborate the theoretical results and the study demonstrates the importance of using a nonlinear model valid within a wide operating range for the design of the stack temperature control, as well as the relevance and advantages of employing a multiobjective optimization methodology to solve this control problem.

The main contributions of this article to the area of temperature control of fuel cell stacks are the followings:

- The design of the temperature control is carried out using a non-linear model which is valid within a wide operating range. This represents an improvement over the use of linearized models valid only around one operating point.
- Control efforts are taken into account in the design of the controller and, therefore, the parasitic consumption of the actuators is incorporated into the design (by means of a multiobjective approach).
- The designed temperature controller is experimentally validated in a real system, which guarantees the theoretical results previously obtained in simulation.

Note that the choice of the control structure adopted in this work (multiloop PID) is a secondary issue in this research. The subject of the article is the control design methodology, *not* a particular control structure. The advantages of this methodology remain, regardless of which control structure is chosen. Thus, a comparison of different control structures is a task that is beyond the scope of this article.

The rest of the article is structured as follows: In section II, we describe the micro-CHP system. In section III, we introduce the nonlinear model of the stack cooling system that serves as the basis for the control design, as well as the modifications carried out in that model. In section IV, we present the methodology followed in this article as well as the control design methodology. In section V, we show the results achieved, both theoretical and experimental. In section VI, we discuss these results. Finally, in section VII we conclude.

II. MICRO-CHP SYSTEM

In this section, we briefly describe the micro-CHP system, paying special attention to the stack cooling system. For a detailed description of the experimental equipment, see [17]. At the end of the article, in Appendix I, the reader will find information about the most relevant devices that constitute the real system, as well as their basic parameters.

Fig. 1 shows the equipment where the experimental tests were conducted. The basic elements of the micro-CHP system are: PEMFC stack, air supply system, hydrogen supply system, electronic load, radiator, hot water tank, stack cooling system, control unit and computer. In the latter, a SCADA is run for plant monitoring and control.

The stack is fed with hydrogen and air, and produces power and heat. The electrical energy is consumed by the electronic load, by means of which we emulate domestic power consumption (lighting and appliances). The thermal energy is stored in the hot water tank, which serves as a heat buffer. Water temperature in this tank is around 55 °C. The thermal energy demand (hot water and heating) is emulated by means of the radiator: when activated it extracts part of the heat stored in the hot water tank.

For the correct operation of the system and to guarantee the safety of the stack, the stack temperature must be maintained within limits. This temperature is measured by a sensor installed in the stack water outlet, whose measurement ($T_{w_{out}}$) is considered as a representative measure of the temperature inside the stack. In addition, according to the stack manufacturer, to achieve optimum electrical efficiency, this temperature must be kept at 65 °C. This value is, therefore, its set point.

On the other hand, the temperature difference between stack outlet water and stack inlet water ($T_{w_{out}} - T_{w_{in}}$) must also be kept within limits to achieve a uniform and limited temperature gradient in the stack. This is necessary to avoid thermal stress in the stack and, consequently, its deterioration. Ideally, according to the stack manufacturer, this temperature gradient should be kept at 5 °C. Therefore, the set point of $T_{w_{in}}$ is programmed at 60 °C.

In order to maintain $T_{w_{out}}$ and $T_{w_{in}}$ at their corresponding set points, a cooling system is used (Fig. 2). Changes in the electrical current demand i (A) will produce undesirable transient fluctuations in the stack temperature ($T_{w_{out}}$) with respect to its optimum value (65 °C), resulting in a loss of electrical efficiency or in a greater deterioration of the stack. The same is true for the hot water tank temperature (T_{t2}): changes in T_{t2} will produce undesirable fluctuations in $T_{w_{in}}$ and, indirectly, in $T_{w_{out}}$. However, the effect of T_{t2} on the stack temperature is less than that produced by changes in the electrical current.

To counteract the effect of the disturbances and keep $T_{w_{out}}$ at its set point, the water flow rate of the primary circuit F_{w_1} (l/min) is varied: if F_{w_1} increases, more heat is removed from the stack and $T_{w_{out}}$ decreases, and vice versa. Similarly, to maintain the stack inlet water temperature ($T_{w_{in}}$) at its set point, the water flow rate of the secondary circuit F_{w_2} (l/min) is varied: if F_{w_2} increases, the amount of heat transferred from the primary to the secondary circuit through the heat exchanger increases (since $T_{t2} < T_{w_{out}}$) and, consequently, $T_{w_{in}}$ decreases; if F_{w_2} decreases, the amount of heat transferred decreases and $T_{w_{in}}$ increases. To vary F_{w_1} a motorized valve is used (pump 1 works at steady state). To vary F_{w_2} a pump is used (pump 2), which is driven by a variable-speed drive.

A temperature control (implemented in the control unit, with a sampling time of 0.1 seconds, and parameterized through the SCADA) is responsible for maintaining $T_{w_{out}}$ and $T_{w_{in}}$ to their set points. This controller acts on the set points of two internal control loops that control the

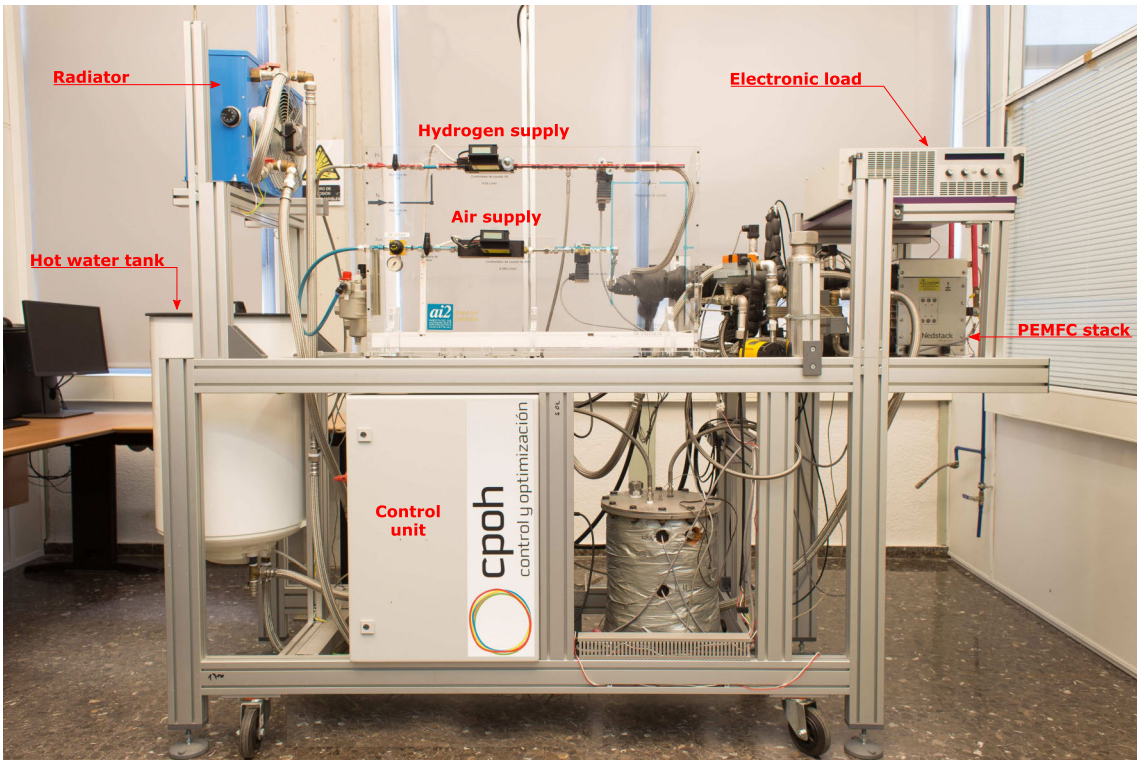

FIGURE 1. Experimental equipment [17].

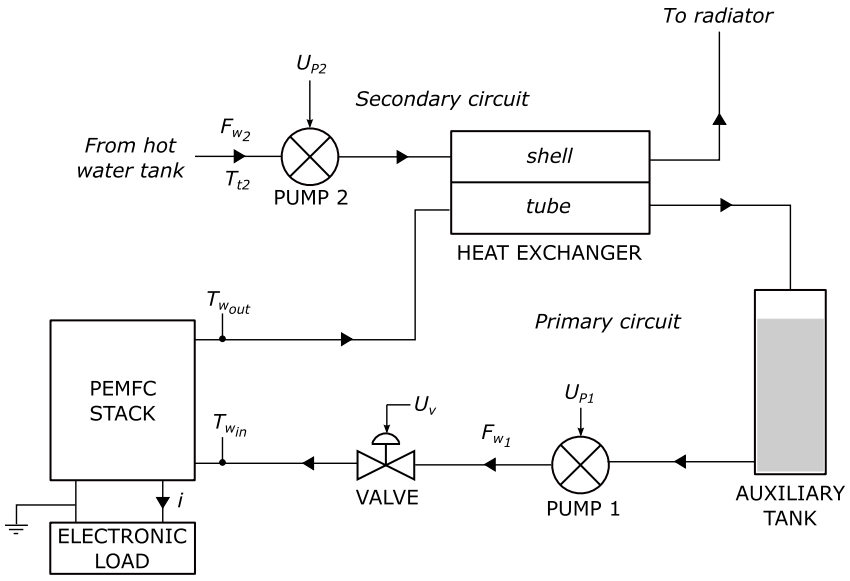

FIGURE 2. Stack cooling system. By means of the water flow rate of the primary circuit F_{w_1} (l/min) the stack temperature $T_{w_{out}}$ (°C) is controlled and by means of the water flow rate of the secondary circuit F_{w_2} (l/min) the stack inlet water temperature $T_{w_{in}}$ (°C) is controlled. Changes in the electrical current demand i (A) will cause undesirable fluctuations in $T_{w_{out}}$.

water flow rates F_{w_1} and F_{w_2} (cascade control configuration). Both internal controllers, the one that controls F_{w_1} and the one that controls F_{w_2}, are PI-type. These controllers are not object of study in this work. The control actions of the temperature control (which are in turn the set points for the internal control loops) are $u_{T_{w_{out}}}$ (l/min) and $u_{T_{w_{in}}}$ (l/min).

The temperature control will have to respond to disturbances in order to minimize the excursions of $T_{w_{out}}$ and $T_{w_{in}}$ from their set points, 65 °C and 60 °C, respectively. This ensures that the stack works at its optimum operating point (maximum electrical efficiency and minimum deterioration). The design of this temperature control is the subject of this article.

III. COOLING SYSTEM MODEL

For the design of the stack temperature control, it has been used a model of the cooling circuit of the micro-CHP system described in the previous section. This model was developed and experimentally validated in [17]. Since it is the starting point for the design of the control that we address here, we will briefly describe its most relevant characteristics.

The model is built in Matlab® and has 30 parameters, all of which represent real physical magnitudes of the plant. Its inputs are: supply air flow rate (F_a), ambient temperature (T_{amb}), supply air temperature ($T_{a_{in}}$), stack voltage (v), electric current supplied by the stack (i), primary circuit water flow rate (F_{w_1}), secondary circuit water flow rate (F_{w_2}) and radiator activation signal (R). And its outputs are: stack water outlet temperature ($T_{w_{out}}$), stack water inlet temperature ($T_{w_{in}}$), water temperature in the hot water tank, i.e. tank 2 (T_{t2}), stack air outlet temperature ($T_{a_{out}}$), water temperature in the heat exchanger shell inlet ($T_{s_{in}}$) and water temperature in the heat exchanger shell outlet ($T_{s_{out}}$). The model is based on first principles, nonlinear, dynamic, and was experimentally validated within a wide operating range (from 140 to 200 A). It is accessible at `http://hdl.handle.net/10251/118336`.

In order to use the nonlinear model in the design of the temperature control, we had to make some modifications to it. These modifications are the following ones.

First, the polarization curve of the stack at $T_{w_{out}}$ equal to 65 °C was included in the model. This polarization curve was obtained experimentally and is shown in Fig. 3. The dynamics of the electrical phenomena are much faster than that of the thermal phenomena, so there was no need to consider them.

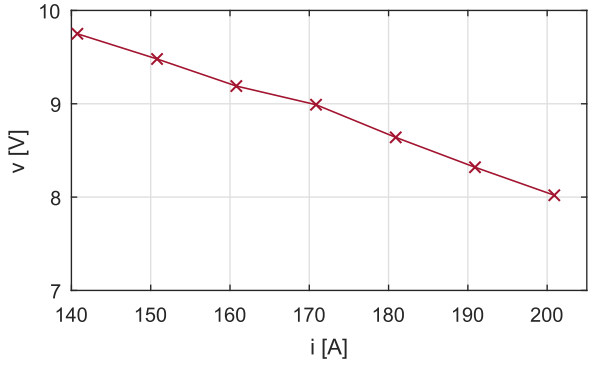

FIGURE 3. Stack polarization curve (experimental data). Stack voltage v as a function of stack current i at $T_{w_{out}}$ equal to 65 °C.

Second, the supply air flow rate (F_a) was calculated according to the equation recommended by the stack manufacturer, which is based on Faraday's law, but modified for a stoichiometry factor of 3 (the value set in the system) instead of 2. In this way: $F_a = 0.796 \cdot i$ (l/min). Dynamics between i and F_a are not considered, since the response of the air supply control is very fast compared to the thermal phenomena and, for this reason, their effect is negligible.

Third, the internal control loops of F_{w_1} and F_{w_2} were modeled and incorporated to the model. These control loops were mentioned in [17] but they were not part of the model. Both control loops have their own dynamics and non-linearities, including: dead zone, backlash, transport delay, nonlinear curves, rate limiter and saturations. Their modeling and inclusion in the model were necessary to achieve a satisfactory experimental validation.

Fourth, a noise with similar characteristics to that of the plant signals and the filters implemented in the system were also included in the model. They are two first-order discrete filters (one for $T_{w_{out}}$ and another for $T_{w_{in}}$) with unity gain and a pole at $z = 0.95$.

Fifth, a slew rate of 20 A/s in the electric current demand was incorporated in the model to represent the one implemented in the real system.

Sixth, ambient temperature (T_{amb}) was set at 30 °C, which is approximately the temperature in the laboratory when the stack has been working at steady state for a while.

Seventh, supply air temperature ($T_{a_{in}}$) was set at 48 °C, also an approximate value of that temperature when the stack works in steady state.

Eighth and last, the model was simplified as follows. In the original model, T_{t2} was a state variable that was provided as an output. Now T_{t2} is considered as constant, with a value of 54.45 °C (middle point of the validity range of the model for this variable). This simplification was made for the following reason: It was assumed that the influence of this signal on the temperatures $T_{w_{out}}$ and $T_{w_{in}}$ was much less than the effect produced by the electric current i, since T_{t2} affects $T_{w_{out}}$ indirectly, through $T_{w_{in}}$, whereas i affects $T_{w_{out}}$ directly. Moreover, there can be abrupt changes (i.e. more disturbing) in the electric current demand but there cannot be such changes in the temperature of the hot water tank. For these reasons, we decided to focus on the control response to changes in the electric current demand and to assume that the temperature T_{t2} remains constant. When T_{t2} is set to a constant value, several elements of the secondary circuit become unnecessary as they no longer have any effect on the operation of the stack. More specifically: the radiator, the hot water tank and pipes 2 and 3. Consequently, these elements were removed from the model.

After making the described modifications, the model is left with two inputs, two outputs and one disturbance. Fig. 4 shows a black box diagram of the model, indicating its inputs and outputs. Remember that $u_{T_{w_{out}}}$ and $u_{T_{w_{in}}}$ are the set points of F_{w_1} and F_{w_2}, respectively (and will be the control actions of the temperature control). This nonlinear model, as noted before, is the starting point for the design of the temperature control.

IV. TEMPERATURE CONTROL DESIGN

A. METHODOLOGY

The methodology followed in this article consists of five stages:

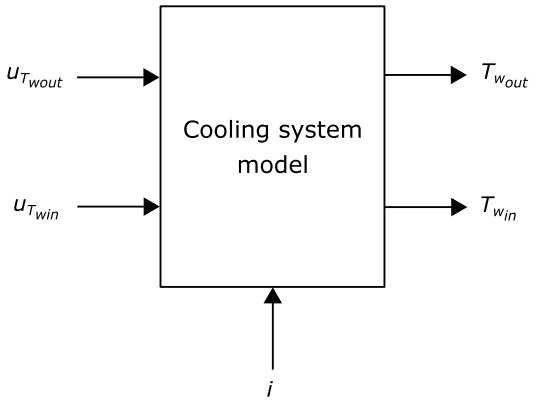

FIGURE 4. Black box diagram of the nonlinear model of the micro-CHP system cooling circuit. After the modifications performed, the model is left with two inputs, two outputs and one disturbance.

1) Obtaining a linear model from the nonlinear model.
2) Design of a temperature control using the *linear model* obtained.
3) Design of a temperature control using the *nonlinear model*.
4) Analysis and comparison of the performance of the two designed controls.
5) Experimental verification of the theoretical results.

Before describing each of these stages it is important to clarify one point. The five stages listed are *the stages followed in this article*, not the stages necessary to design a PEMFC stack temperature controller. Certainly, these five stages include the necessary tasks to design a temperature controller from a nonlinear model using multiobjective optimization, but they also include other stages that are not necessary for that design. Properly speaking, the methodology *for the design of the temperature control* that we propose is the one shown in Fig. 5. This methodology corresponds to stages 3 and 5. The rest of the stages of the methodology followed in this article are auxiliary (stages 1, 2 and 4). The aims of these auxiliary stages are 1) to demonstrate the inadequacy of using a linear model in the design of a PEMFC stack temperature control, and 2) to show, by comparison, that the results achieved using a nonlinear model are superior to those achieved using a linear model.

In stage 1, a linear model is obtained from the nonlinear model described in the previous section. For this purpose, a virtual test (in simulation, using the nonlinear model) was carried out. This procedure is for all purposes equivalent to a test on the real plant, by which the linear model could also have been obtained. In this test, step signals were applied (independently and sequentially) to the inputs $u_{T_{w_{out}}}$ and $u_{T_{w_{in}}}$, and to the disturbance i. The test was carried out at an operating point, namely, $T_{w_{out}} = 65$ °C, $T_{w_{in}} = 60$ °C, $i = 170$ A, $u_{T_{w_{out}}} = 4.43$ l/min and $u_{T_{w_{in}}} = 4.99$ l/min. These values for the control actions are the ones that keep both temperatures stable at their set points when $i = 170$ A. This operating point corresponds to the middle point of the

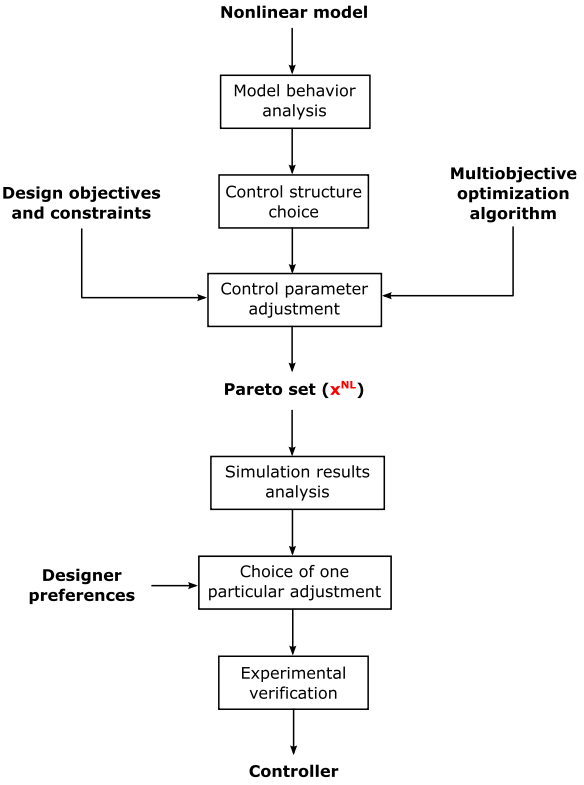

FIGURE 5. Control flow diagram of the methodology for the design of the PEMFC stack temperature controller. This control flow diagram corresponds to the stages 3 and 5 (partially) of the methodology followed in this article.

validity ranges of the nonlinear model. The amplitudes of the steps were set so that the discrepancy between the response of the linearized model and that of the nonlinear model (for each excitation) was less than 10%. This resulted in amplitudes for the step signals of: ±0.1 l/min for $u_{T_{w_{out}}}$, ±0.1 l/min for $u_{T_{w_{in}}}$, ±1 A for i. Finally, with the signals from this virtual test and using the System Identification Toolbox™ of Matlab®, we obtained the transfer functions of the linearized model, which is a 2 × 3 MIMO model, valid around the specified operating point:

$$\begin{bmatrix} T_{w_{out}} \\ T_{w_{in}} \end{bmatrix} = \begin{bmatrix} G_{11} & G_{12} & G_{13} \\ G_{21} & G_{22} & G_{23} \end{bmatrix} \begin{bmatrix} u_{T_{w_{out}}} \\ u_{T_{w_{in}}} \\ i \end{bmatrix} \tag{1}$$

$$G_{11}(s) = \frac{-0.942}{1 + 24.0s} e^{-41.6s} \tag{2}$$

$$G_{12}(s) = \frac{-0.741(1 + 354.0s)}{(1 + 438.7s)(1 + 72.7s)(1 + 13.2s)} e^{-7.7s} \tag{3}$$

$$G_{13}(s) = \frac{0.092(1 + 258.9s)}{(1 + 336.1s)(1 + 47.3s)} \tag{4}$$

$$G_{21}(s) = \frac{0.196(1 + 104.6s)}{1 + 2{\cdot}0.934{\cdot}34.1s + (34.1s)^2} e^{-41.1s} \tag{5}$$

$$G_{22}(s) = \frac{-0.772(1 + 358.9s)}{(1 + 409.8s)(1 + 68.9s)(1 + 3.1s)} e^{-3.8s} \tag{6}$$

$$G_{23}(s) = \frac{0.050}{1 + 133.6s} \tag{7}$$

Stages 2 and 3 will be discussed together. In each of these stages, a control is designed. Both designs are identical, except that in the first the linear model is used and in the second the nonlinear model is used. We will call the control designed in stage 2 C_L and the one designed in stage 3 C_{NL}. The subscripts L and NL refer to the model used in the design of each control (linear model or nonlinear model).

The control structure of C_L and C_{NL} is the same: two PI-type controllers with anti-windup, one for the control of $T_{w_{out}}$ and the other for the control of $T_{w_{in}}$ (see Fig. 6). The equation of the PI-type controllers is formulated in the standard form (see equation 8). The derivative actions were switched off to avoid amplifying the measurement noise and thus protecting the actuators (on this point see also IV-B). Therefore, each control (C_L and C_{NL}) has four parameters to adjust (two for each PI), namely K_{c1} ((l/min)/°C), K_{c2} ((l/min)/°C), T_{i1} (s) and T_{i2} (s). These parameters are adjusted by solving a multiobjective optimization problem (MOP).

$$u(t) = K_c \left[e(t) + \frac{1}{T_i} \int e(t)dt \right] \tag{8}$$

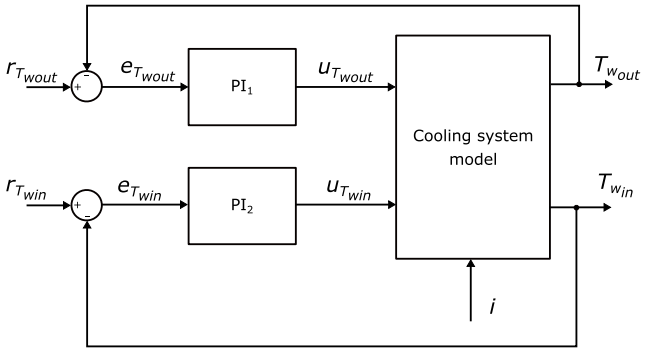

FIGURE 6. Control structure adopted in the design of controls C_L and C_{NL}.

The process of solving a multiobjective optimization problem (a posteriori) consists of three basic stages [24]: 1) problem definition (objectives, decision variables, constraints), 2) optimization (optimal solutions search) and 3) multicriteria decision-making (choice of the final solution by the designer). It is important to note that for each control (C_L and C_{NL}) the optimization will not provide a single optimal solution, but a set of optimal solutions called Pareto set. We will call the solutions of C_L $\boldsymbol{x}^L$ and the solutions of C_{NL} $\boldsymbol{x}^{NL}$. All the solutions in a Pareto set are optimal. This means that none of the solutions in a Pareto set is better than another in the same set for all the objectives. Note that each of these optimal solutions is properly a controller, i.e. a certain adjustment of the parameters of the two PI controllers that constitute the control structure. Thus, from now on we will refer to ''solutions'' as well as ''controllers''.

The a posteriori multiobjective optimization methodology has the following advantage: in the final decision-making stage, the designer knows all the optimal solutions and can therefore compare them directly. This allows them to analyze the trade-off between the different solutions of the Pareto set and, in this way, to choose one of them knowing all the relevant information, which increases the designer's confidence that the final chosen solution is the correct one. The formulation of the multiobjective optimization problem, i.e. objectives and constraints, as well as the optimization algorithm used, will be described in section IV-B.

The adjustment of the parameters of both PI controllers is carried out simultaneously. This is important, because due to the very nature of the process there is a strong coupling between the control actions and the outputs: $u_{T_{wout}}$ affects both $T_{w_{out}}$ and $T_{w_{in}}$, and $u_{T_{win}}$ affects both $T_{w_{in}}$ and $T_{w_{out}}$. By simultaneously adjusting both PI controllers, these coupling effects are taken into account implicitly in the design of the control.

As indicated above, the temperature control should be able to respond to changes in the electric current demand i. The electric current demand signal used for the design of the controls (C_L and C_{NL}) is shown in Fig. 7. The choice of this signal is important. It has to represent the worst case (abrupt steps) and travel throughout the entire validity range of the nonlinear model (from 140 to 200 A).

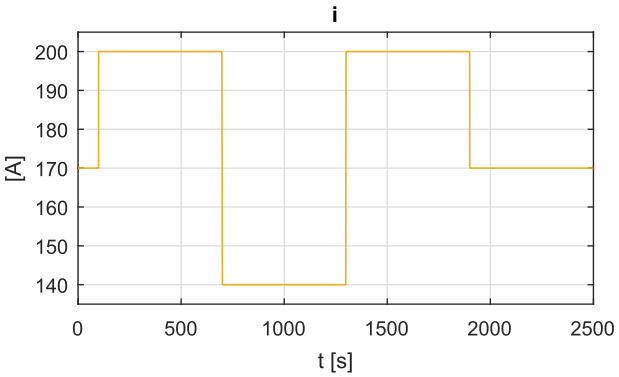

FIGURE 7. Electric current demand signal used in the design of the controls. The first step is applied at t=100 s and the span of each step is 600 s, so changes occur in 100, 700, 1300 and 1900 seconds.

In stage 4 (analysis and comparison of the performances of C_L and C_{NL}), two comparisons are carried out, namely:

A) Performance of the solutions of C_L when simulated using the linear model versus performance of the same solutions when simulated using the nonlinear model (see Fig. 8).

B) Performance of the solutions of C_L when simulated using the nonlinear model versus performance of the solutions of C_{NL} when simulated using the nonlinear model (see Fig. 9).

Finally, in stage 5, the experimental verification of the theoretical results is conducted. In this stage, the theoretical results (the simulations with the nonlinear model carried out in stage 4) are compared with the experimental results (tests on the real process). We call this third comparison ''comparison C'' (see Fig. 9).

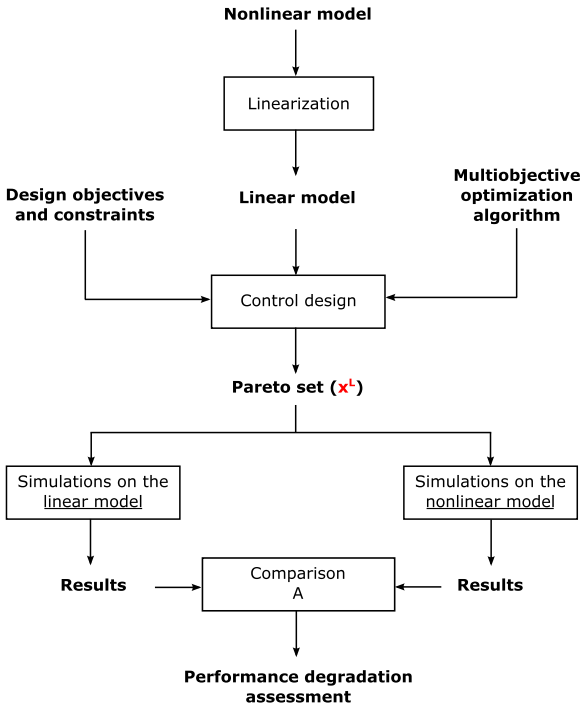

FIGURE 8. Control flow diagram of the auxiliary tasks undertaken to assess the performance degradation of the control C_L. This control flow diagram corresponds to the stages 1, 2 and 4 (partially) of the methodology followed in this article.

Therefore, three types of fundamental comparisons are performed (comparisons A, B and C). These three comparisons will be presented in section V, each of them in a separate subsection.

B. MOP. DESIGN OBJECTIVES, CONSTRAINTS AND FORMULATION

In section II, two important design objectives were already mentioned, namely, maintaining $T_{w_{out}}$ and $T_{w_{in}}$ at their set points (65 °C and 60 °C, respectively). The aim of these two objectives is to achieve an optimal electrical efficiency and a minimal deterioration of the stack.

Apart from minimizing the errors of the outputs with respect to their set points, there is another fundamental aspect that must be taken into account in the design of the control, namely: control efforts. This is so for two reasons. First, because the power consumption of the actuators (which depends on the control efforts) reduces the global electrical efficiency of the system. Second, because the lifetime of the actuators (valves, pumps) can be significantly reduced if they are exposed to very aggressive control actions. Consequently, control efforts will be incorporated into the MOP by means of two additional objectives.

Note that the problem of designing the temperature control of a PEMFC stack includes several conflicting objectives. For this reason, the multiobjective optimization methodology is especially appropriate for this task.

In the design we also included a constraint regarding the settling times of $T_{w_{out}}$ and $T_{w_{in}}$, namely, all the responses that did not reach stabilization at t=600 s (since the change in i) were discarded. For this we defined a threshold.

Once objectives and constraints have been chosen, it is possible to formulate the control design as a multiobjective optimization problem, as follows:

$$\min_{\boldsymbol{x}} \boldsymbol{f}(\boldsymbol{x}) \tag{9}$$

where:

$$\boldsymbol{f}(\boldsymbol{x}) = \left[f_1(\boldsymbol{x})\ f_2(\boldsymbol{x})\ f_3(\boldsymbol{x})\ f_4(\boldsymbol{x})\right] \tag{10}$$

and

$$\boldsymbol{x} = \left[K_{c1}\ K_{c2}\ T_{i1}\ T_{i2}\right] \tag{11}$$

subject to:

$$\underline{\boldsymbol{x}} \leq \boldsymbol{x} \leq \overline{\boldsymbol{x}} \tag{12}$$

$$\underline{\boldsymbol{x}} = \left[-5\ -5\ 1\ 1\right] \tag{13}$$

$$\overline{\boldsymbol{x}} = \left[-0.1\ -0.1\ 100\ 100\right] \tag{14}$$

The mathematical formulation of the four objectives is:

$$f_1(\boldsymbol{x}) = \frac{1}{T_{sim}} \int_0^{T_{sim}} \left| e_{T_{w_{out}}}(t) \right| dt \tag{15}$$

$$f_2(\boldsymbol{x}) = \frac{1}{T_{sim}} \int_0^{T_{sim}} \left| e_{T_{w_{in}}}(t) \right| dt \tag{16}$$

$$f_3(\boldsymbol{x}) = \frac{1}{T_{sim}} \int_0^{T_{sim}} \left| \frac{du_{T_{w_{out}}}(t)}{dt} \right| dt \tag{17}$$

$$f_4(\boldsymbol{x}) = \frac{1}{T_{sim}} \int_0^{T_{sim}} \left| \frac{du_{T_{w_{in}}}(t)}{dt} \right| dt \tag{18}$$

The objective f_1 is the average absolute error in the stack temperature $T_{w_{out}}$, in °C. The objective f_2 is the average absolute error in stack inlet water temperature $T_{w_{in}}$, in °C. The objective f_3 is the average absolute value of the rate of change of the control action $u_{T_{w_{out}}}$, in (l/min)/s. The objective f_4 is the average absolute value of the rate of change of the control action $u_{T_{w_{in}}}$, in (l/min)/s. T_{sim} is the simulation time (2500 s).

The settling time requirement is formulated as:

$$\left| e_{T_{w_{out}}}(100 + 600n - \epsilon) \right| < 0.033\ ^\circ C \tag{19}$$

$$\left| e_{T_{w_{in}}}(100 + 600n - \epsilon) \right| < 0.033\ ^\circ C \tag{20}$$

For $n = 1, 2, 3, 4$ and $\epsilon = [0\ \ 10]$ s, i.e. for the four ten-second time intervals preceding the steps in the electric current demand (except for the first step at 100 s).

Note that in the MOP formulation, the objectives have been defined and quantified independently, i.e. we avoid aggregating objectives to simplify the problem (for example, globally quantifying control effort as the sum of f_3 and f_4). This prevents the optimization algorithm from ruling out relevant solutions that are nearly optimal solutions in the aggregate formulation. For this question see [21].

In order to prevent the noises in the control actions from distorting the calculation of the control efforts (f_3 and f_4),

the optimization was run without noise. The noise level in the control actions, on the other hand, was indirectly limited by the maximum values of K_{c1} and K_{c2}, -5 (l/min)/°C, which are the gains of the PI controllers at high frequency.

The optimization algorithm used for the search of the optimal solutions is evMOGA [25], available at https://www.mathworks.com/matlabcentral/fileexchange/31080-ev-moga-multiobjective-evolutionary-algorithm.

The algorithm is run in Matlab®. The values for the parameterization of the algorithm are: $N_{indP} = 400$ (number of individuals in the main population), $N_G = 1000$ (number of generations), $n_{div} = 50$ (number of divisions for each dimension). With this configuration, the algorithm evaluates the objective functions 4400 times.

The same objectives, constraints and evMOGA parameterization were used for all optimization runs.

V. RESULTS

Table 1 lists the parameter optimization results obtained using the linear model, i.e. the optimal solutions of C_L (10 solutions). Table 2 lists the parameter optimization results obtained using the nonlinear model, i.e. the optimal solutions of C_{NL} (21 solutions).

TABLE 1. Parameter optimization results obtained using the linear model, i.e. solutions of C_L.

$\boldsymbol{x}^L$	K_{c1}	K_{c2}	T_{i1}	T_{i2}
1	−0.27	−1.90	58.1	87.9
2	−0.83	−0.71	76.0	33.8
3	−0.62	−3.03	59.9	55.4
4	−0.24	−1.22	39.1	43.4
5	−0.77	−2.11	58.7	73.1
6	−0.25	−2.12	27.0	6.8
7	−0.39	−3.94	44.7	86.1
8	−0.45	−4.23	55.8	57.5
9	−1.07	−0.60	70.3	24.5
10	−0.26	−4.19	37.5	47.3

TABLE 2. Parameter optimization results obtained using the nonlinear model, i.e. solutions of C_{NL}.

$\boldsymbol{x}^{NL}$	K_{c1}	K_{c2}	T_{i1}	T_{i2}
1	−1.05	−2.90	77.4	44.4
2	−1.62	−1.20	26.9	64.4
3	−1.28	−4.86	96.9	59.7
4	−0.92	−2.13	67.0	60.3
5	−2.55	−1.61	97.5	61.4
6	−0.51	−3.86	19.0	85.9
7	−0.94	−3.77	24.6	96.7
8	−1.91	−1.72	47.2	68.1
9	−0.87	−3.81	66.5	95.2
10	−1.78	−1.81	26.6	71.5
11	−0.89	−1.89	21.0	85.4
12	−1.68	−2.41	23.9	72.4
13	−1.29	−3.38	87.6	28.2
14	−1.02	−1.57	58.1	60.0
15	−1.26	−3.27	78.5	25.5
16	−0.69	−2.65	75.1	89.1
17	−0.68	−3.81	32.3	71.8
18	−0.62	−3.03	70.9	83.2
19	−0.78	−2.10	57.5	47.3
20	−0.32	−4.43	32.5	80.6
21	−0.86	−1.72	24.0	69.9

A first observation, before even looking at the values of the objective functions for the solutions of C_L and C_{NL}, is the following. If we consider (as an approximation) the static gains of the controllers as indicators of how aggressive they are (which can be done, since there is no derivative action), it turns out that, on average, the controllers of C_{NL} are more aggressive than those of C_L. In particular, the PI controller of $T_{w_{out}}$ (PI_1) is 2.17 times more aggressive and the PI controller of $T_{w_{in}}$ 1.15 times. This means that the controllers of C_L are unnecessarily conservative and, for this reason (as we will see in this section), they will not achieve a superior performance, which the controllers of C_{NL} do achieve.

For the graphic representation of the solutions, a multidimensional visualization tool called *level diagrams* has been used [22], [23]. This tool is available at: https://www.mathworks.com/matlabcentral/fileexchange/62-224-interactive-tool-for-decision-making-in-multiobjective-opti-mization-with-level-diagrams. In level diagrams, each objective and each parameter is represented in a separate diagram. The diagrams of the objectives will be placed to the left of the figures and those of the parameters to the right. In the diagrams of the objectives the x-axis represents the value of each objective function, whereas in the diagrams of the parameters the x-axis represents the value of each parameter. In all diagrams (objectives and parameters), the y-axis represents the value of a norm.

There are different norms (1-norm, 2-norm, ∞-norm). We have chosen 2-norm. 2-norm measures the Euclidean distance (in the space of the objectives rescaled between 0 and 1) of a solution to the ideal or utopian point (in this case, [0 0 0 0]). That is to say, the value of the 2-norm for a solution $\boldsymbol{x}_i$ is:

$$\|\boldsymbol{f}(\boldsymbol{x}_i)\|_2 = \sqrt{\sum_{k=1}^{4} f'_k(\boldsymbol{x}_i)^2} \tag{21}$$

where f'_k is f_k rescaled between 0 and 1, for $k = 1 \ldots 4$.

The diagrams are synchronized: when a solution is selected in any of them, that same solution is selected in the rest of the diagrams. Fig. 10 represents in level diagrams: 1) the set of solutions of C_L (green), 2) these same solutions simulated using the nonlinear model (red) and 3) the set of solutions of C_{NL} (purple). This color coding will be used also to represent the dynamic responses of the controlled system.

In Fig. 10, the representation in level diagrams provides, for each solution: 1) the value of the parameters of that solution (in the four diagrams on the right, x-axis) and 2) the value of the objectives for that solution (in the four diagrams on the left, x-axis). As well as the value of its 2-norm (y-axis in all diagrams). This means that each solution $\boldsymbol{x}_i$ is represented by eight points. Each of these points is plotted on a different diagram (there are eight diagrams). If we call $\mathcal{N}_i$ to $\|\boldsymbol{f}(\boldsymbol{x}_i)\|_2$ (see equation 21), then the eight points are:

$$\begin{array}{cccc} (f_1(\boldsymbol{x}_i), \mathcal{N}_i) & (f_2(\boldsymbol{x}_i), \mathcal{N}_i) & (K_{c1}, \mathcal{N}_i) & (K_{c2}, \mathcal{N}_i) \\ (f_3(\boldsymbol{x}_i), \mathcal{N}_i) & (f_4(\boldsymbol{x}_i), \mathcal{N}_i) & (T_{i1}, \mathcal{N}_i) & (T_{i2}, \mathcal{N}_i) \end{array} \tag{22}$$

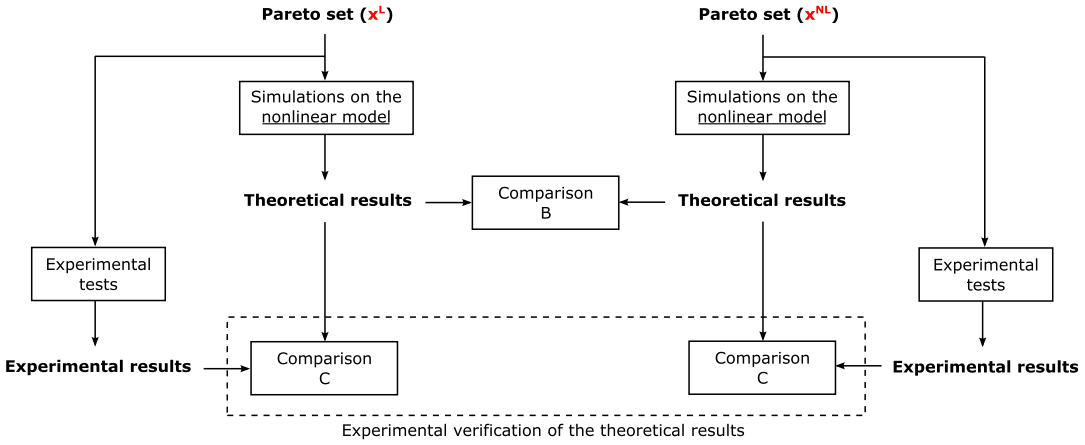

FIGURE 9. Control flow diagram of the auxiliary tasks undertaken 1) to compare the performances of C_L and C_{NL} and 2) to verify experimentally the theoretical results obtained in simulation. This control flow diagram corresponds to the stages 4 (partially) and 5 of the methodology followed in this article.

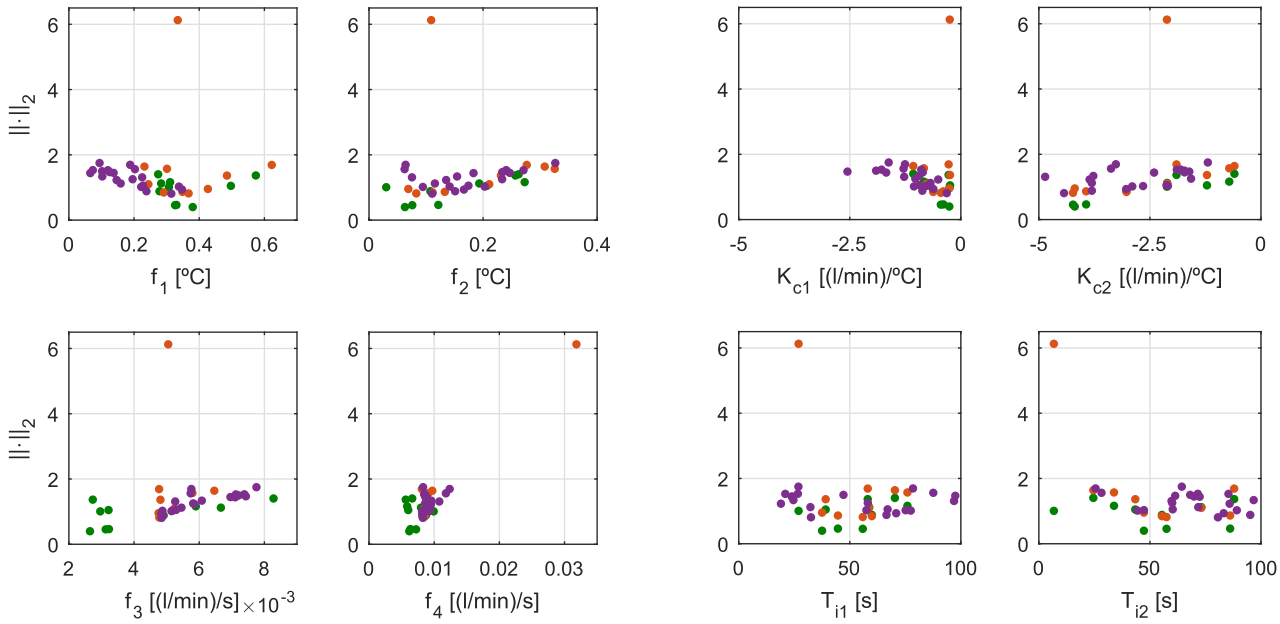

FIGURE 10. Representation in level diagrams of the 10 solutions of C_L, simulated using the linear model (green) and simulated using the nonlinear model (red), and of the 21 solutions of C_{NL} simulated using the nonlinear model (purple). The four diagrams on the left show the four objectives of the MOP and the four diagrams on the right show the four decision variables (parameters).

where K_{c1}, K_{c2}, T_{i1} and T_{i2} are the values of the parameters of solution $\boldsymbol{x}_i$ (see equation 11). Note that the value of the y-axis is the same at all points, namely $\mathcal{N}_i$ (the value of 2-norm). Thus, the eight points corresponding to solution $\boldsymbol{x}_i$ are plotted at the same height in the eight diagrams. For a more detailed description of this tool (level diagrams), please see [22], [23] and the online tutorials provided at the above-mentioned URL.

In the following three subsections, the results of stages 4 and 5 are presented. Each of them corresponds to one of the three comparisons mentioned in subsection IV-A (comparisons A, B and C).

A. PERFORMANCE DEGRADATION OF THE SOLUTIONS OF C_L

Table 3 shows the values of the four objectives for each of the ten solutions of C_L, in two scenarios: 1) when these solutions are simulated using the linear model (columns 2-5) and 2) when they are simulated using the nonlinear model (columns 6-9). It also shows the percentage change in the objectives (columns 10-13) and the average percentage change (column 14).

5 out of the 10 solutions ($\boldsymbol{x}_1^L, \boldsymbol{x}_6^L, \boldsymbol{x}_7^L, \boldsymbol{x}_8^L, \boldsymbol{x}_{10}^L$) degrade for all the objectives. This represents 50% of the solutions. The global average degradation of the solutions of C_L is 30.14%.

TABLE 3. Values of the objective functions for the solutions of C_L in two scenarios: simulated using the linear model (columns 2-5) and simulated using the nonlinear model (columns 6-9). Columns 10-13 contain the percentage change for each objective and column 14 the average percentage change. If a controller performance degrades when simulated using the nonlinear model, it is indicated in red, and if it improves in green.

$\boldsymbol{x}^L$	f_1	f_2	$f_3(\times 10^{-3})$	$f_4(\times 10^{-3})$	f_1	f_2	$f_3(\times 10^{-3})$	$f_4(\times 10^{-3})$	Δf_1	Δf_2	Δf_3	Δf_4	$\Delta \bar{f}$
1	0.574	0.257	2.734	5.633	0.623	0.277	4.768	8.105	8.5	7.8	74.4	43.9	33.7
2	0.311	0.273	5.894	5.857	0.301	0.326	5.791	9.144	−3.1	19.3	−1.7	56.1	17.7
3	0.278	0.108	4.908	8.722	0.291	0.112	4.823	8.515	4.7	3.8	−1.7	−2.4	1.1
4	0.497	0.206	3.218	6.019	0.485	0.231	4.810	8.763	−2.4	12.0	49.5	45.6	26.2
5	0.283	0.193	6.665	7.979	0.244	0.211	5.241	8.454	−13.9	9.0	−21.4	6.0	−5.1
6	0.307	0.030	2.964	9.927	0.334	0.109	5.049	31.827	8.9	261.5	70.4	220.6	140.4
7	0.330	0.122	3.230	6.354	0.349	0.133	4.844	8.191	5.6	9.3	50.0	28.9	23.4
8	0.326	0.076	3.130	7.218	0.367	0.083	4.774	8.289	12.7	9.2	52.5	14.8	22.3
9	0.274	0.262	8.281	6.633	0.232	0.308	6.463	9.709	−15.4	17.4	−21.9	46.4	6.6
10	0.380	0.063	2.648	6.180	0.427	0.069	4.753	8.625	12.3	9.4	79.5	39.5	35.2

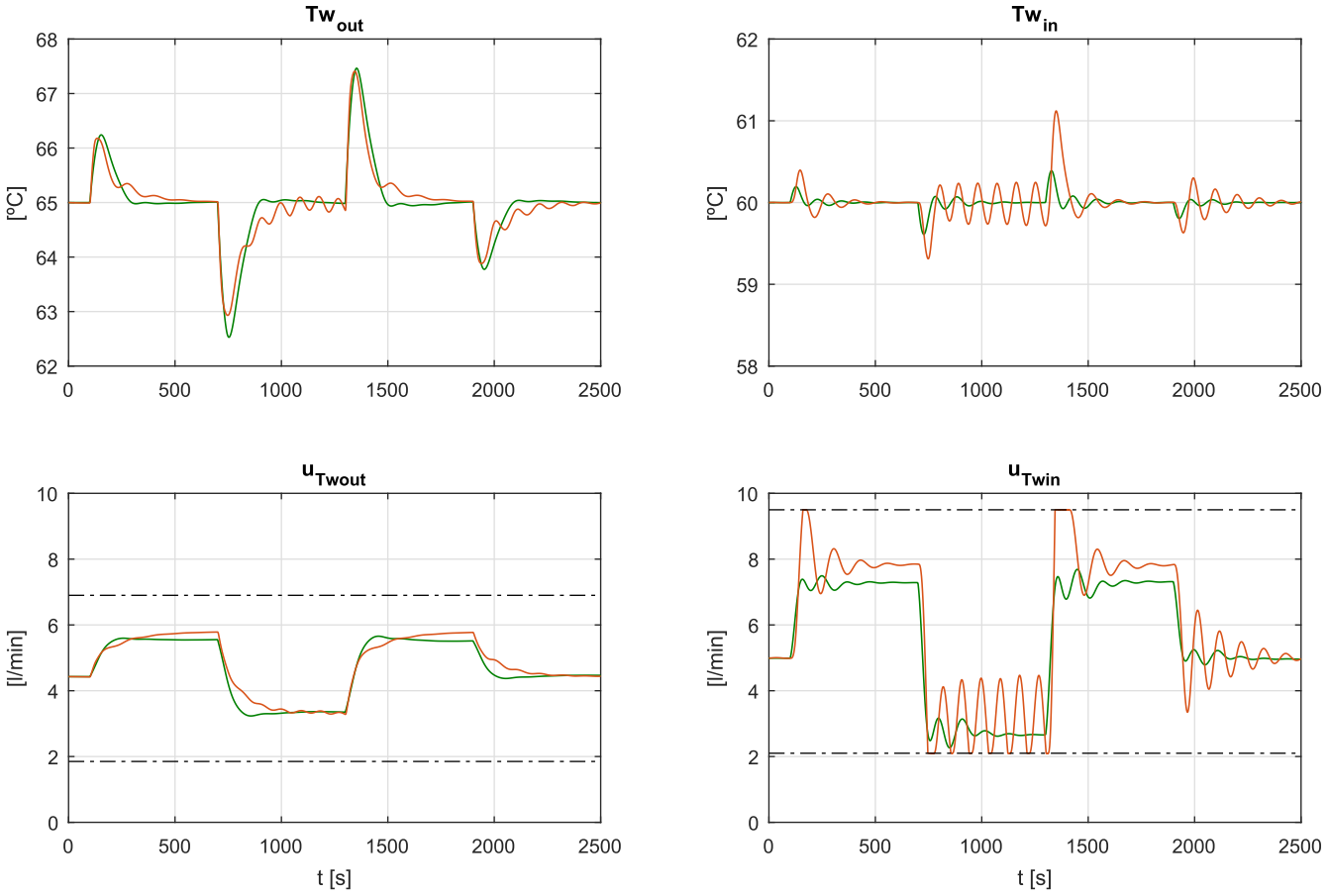

FIGURE 11. Dynamic response of the system controlled by x_6^L, in two scenarios: 1) simulated using the linear model (green) and 2) simulated using the nonlinear model (red).

Moreover, 7 out of the 10 solutions (70%) suffer an average degradation in their performance greater than 17%. It can be stated (in this case), therefore, that the performance of the controllers generally worsens when the solutions obtained using the linear model are tested against the nonlinear model (which represents the real plant).

The solution that degrades the most is $\boldsymbol{x}_6^L$, with an average degradation of 140.35%. The performance degradation suffered by the solution $\boldsymbol{x}_6^L$ is such that the real response of the system controlled by it does not stabilize. This means that solution $\boldsymbol{x}_6^L$ (optimal solution when designing the control using the linear model and, consequently, a solution that could have been chosen by the designer) is, in fact, completely unacceptable, since when it is simulated using the nonlinear model (which represents the real plant), it produces a dynamic response that never stabilizes. It also turns out that solution $\boldsymbol{x}_6^L$, which was the one that provided the best performance for objective f_2 (0.030 °C), is the solution that degrades the most for that same objective (261.52%). Fig. 11 shows the response of the system controlled by $\boldsymbol{x}_6^L$ and Fig. 12 shows the degradation of its performance in level diagrams.

Solution $\boldsymbol{x}_{10}^L$, which is the most balanced solution of C_L (lowest value of 2-norm) and, therefore, a compromise solution highly susceptible of being chosen by the designer,

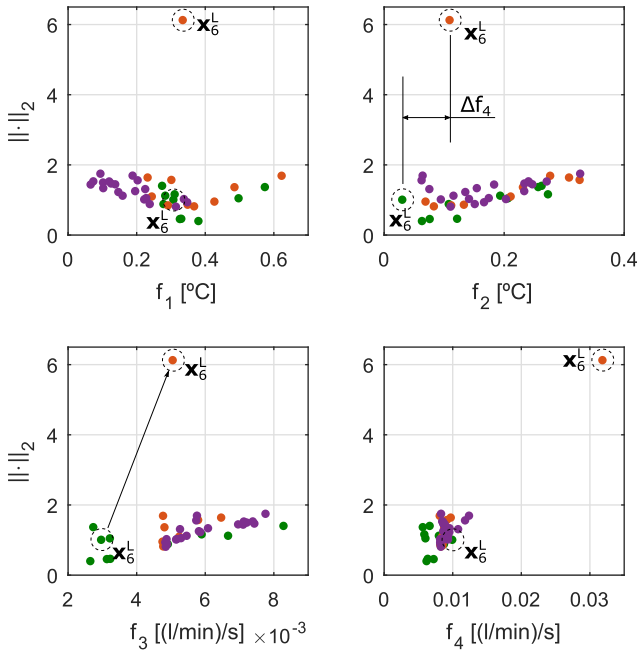

FIGURE 12. Level diagrams representation of the values of the objective functions for the solution x_6^L, in two scenarios: 1) when controlling the linear model (green) and 2) when controlling the nonlinear model (red). The performance achieved by the controller x_6^L degrades for all four design objectives.

degrades for the four objectives, with an average degradation of 35.19%. In particular, the objective f_1 (on which the stack electrical efficiency depends) degrades 12.26%. This can be seen in Fig. 13, which shows the dynamic response ($T_{w_{out}}$) of the system controlled by $\boldsymbol{x}_{10}^L$.

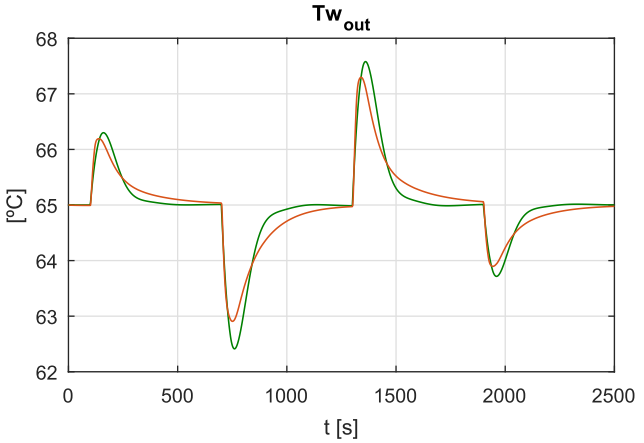

FIGURE 13. Dynamic response ($T_{w_{out}}$) of the system controlled by x_{10}^L, in two scenarios: 1) simulated using the linear model (green) and 2) simulated using the nonlinear model (red). The performance of controller x_{10}^L degrades 12.26% for f_1 (average absolute error in stack temperature).

As can be seen in Fig. 13, solution $\boldsymbol{x}_{10}^L$ produces (when simulated using the nonlinear model) a lower peak value in $T_{w_{out}}$ than when it is simulated using the linear model. Note, however, that the relevant design objective is not the peak value, but f_1, since the stack electrical efficiency is determined by f_1, not by the peak value.

Moreover, solution $\boldsymbol{x}_{10}^L$ fails to meet the design requirement regarding the settling time (see equations 19 and 20). Apart from solution $\boldsymbol{x}_{10}^L$, also $\boldsymbol{x}_1^L, \boldsymbol{x}_4^L, \boldsymbol{x}_6^L, \boldsymbol{x}_8^L$ and $\boldsymbol{x}_9^L$ fail to meet that same design requirement. The solution in which this fact is most appreciable is $\boldsymbol{x}_1^L$ (see Fig. 14).

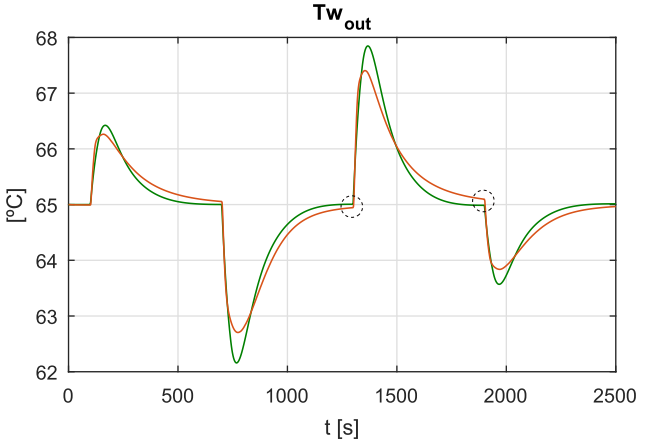

FIGURE 14. Solution x_1^L, which met the settling time requirement when simulated using the linear model (green), fails to meet it when simulated using the nonlinear model (which represents the real plant) (red).

B. COMPARISON OF THE SOLUTIONS OF C_L WITH THOSE OF C_{NL}

Table 4 lists the values of the four objectives for the 21 solutions obtained using the nonlinear model, i.e. for the 21 solutions of C_{NL}.

TABLE 4. Values of the 4 objective functions for the 21 solutions of C_{NL}.

$\boldsymbol{x}^{NL}$	f_1	f_2	$f_3(\times 10^{-3})$	$f_4(\times 10^{-3})$
1	0.222	0.094	5.150	9.312
2	0.094	0.327	7.756	8.297
3	0.225	0.075	5.264	10.785
4	0.228	0.174	5.293	8.712
5	0.125	0.234	7.432	8.637
6	0.147	0.135	5.855	9.505
7	0.102	0.154	6.080	9.536
8	0.102	0.242	7.211	8.656
9	0.238	0.151	4.887	8.210
10	0.073	0.240	7.385	8.473
11	0.120	0.271	7.124	8.527
12	0.066	0.183	7.105	8.862
13	0.203	0.062	5.737	11.797
14	0.196	0.233	5.815	8.616
15	0.188	0.064	5.758	12.373
16	0.338	0.203	4.871	8.156
17	0.159	0.116	5.456	9.322
18	0.347	0.166	4.834	8.168
19	0.227	0.141	5.175	9.024
20	0.314	0.111	4.848	8.263
21	0.137	0.247	6.959	8.672

A comparison of the Tables 3 (columns 6-9) and 4 shows that the vast majority of the solutions of C_{NL} (17 out of 21, 81%) surpass in f_1 the best solution of C_L for that same

objective (x_9^L). This can also be seen in Fig. 16 (in the diagram of f_1).

Solution x_9^L is the one that has the best f_1 when it is simulated using the linear model (0.274 °C) and it is also the one that provides the better f_1 (0.232 °C) when the control of the nonlinear model is simulated (in fact it does not degrade, but improves for that objective). Even so, the value of f_1 at x_{12}^{NL} (0.066 °C), which is the best solution of C_{NL} for that objective, is less than the value of f_1 at x_9^L by 71.65%. Fig. 15 shows the dynamic responses ($T_{w_{out}}$) of the system controlled by x_9^L and by x_{12}^{NL} when simulated using the nonlinear model. Fig. 16 shows this same result in level diagrams.

Here it is interesting (and can be useful for other researchers) to specify the performance achieved by the solution x_{12}^{NL} (temperature overshoot and settling time). These can be taken as conformance values for a continuously improved benchmark for future control scheme developments of fuel cell stacks. Thus, for the third step in the electric current (from 140 A to 200 A, worst case), the solution x_{12}^{NL} achieves a maximum overshoot of 1.05 °C and a settling time (for an error band of 0.1 °C) of 80 seconds.

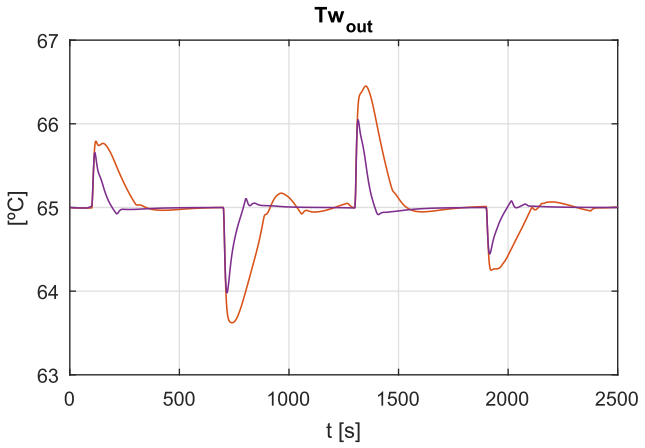

FIGURE 15. Comparison of the dynamic response ($T_{w_{out}}$) of the nonlinear model controlled by the best controller of C_L for f_1 (x_9^L, red) and by the best controller of C_{NL} for that same objective (x_{12}^{NL}, purple). The controller x_{12}^{NL} surpasses x_9^L in f_1 by 71.65%.

Note that some of the solutions obtained as optimal using the linear model are not really optimal solutions (x_2^L, x_5^L, x_9^L). This means that there are solutions among those obtained using the nonlinear model that dominate (they are better for all the objectives) these three solutions. To be exact, solutions $x_1^{NL}, x_4^{NL}, x_6^{NL}, x_7^{NL}, x_9^{NL}, x_{14}^{NL}, x_{17}^{NL}, x_{19}^{NL}$. Each of these solutions of C_{NL} dominates one or more of the three solutions of C_L mentioned. Here are three examples (see numerical values in Table 5):

1) x_1^{NL} is better than x_9^L for all the objectives.
2) x_9^{NL} is better than x_5^L and x_2^L for all the objectives.
3) x_7^{NL}, which is the one of the set considered that has the best f_1, is better than x_9^L for all the objectives.

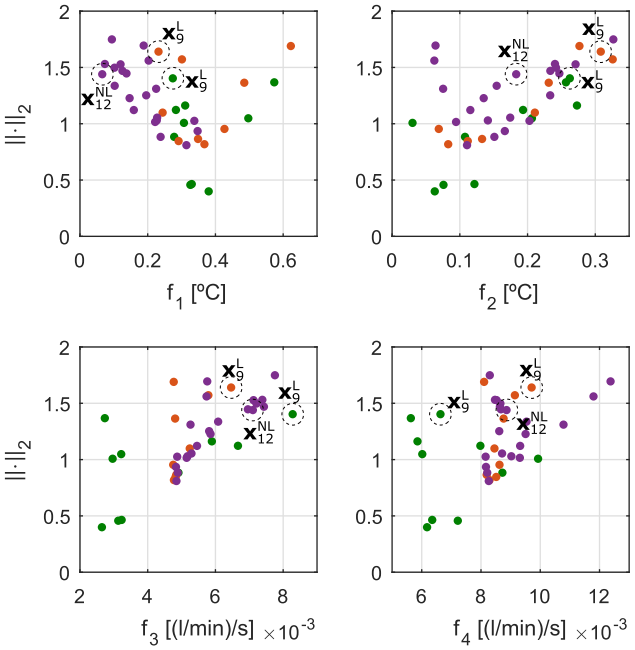

FIGURE 16. Representation of the values of the objective functions in level diagrams. In green, solutions of C_L simulated using the linear model; in red, solutions of C_L simulated using the nonlinear model; and in purple, solutions of C_{NL} simulated using the nonlinear model. The vast majority of the solutions of C_{NL} (17 out of 21, 81%) surpass in f_1 the best solution of C_L for that same objective (x_9^L). The best solution of C_{NL} for f_1 (x_{12}^{NL}) surpasses the best solution of C_L for that same objective (x_9^L) by 71.65%.

TABLE 5. The solutions x_2^L, x_5^L and x_9^L of C_L are not optimal solutions, because they are dominated by one or more solutions of C_{NL}.

	x	f_1	f_2	$f_3(\times 10^{-3})$	$f_4(\times 10^{-3})$
C_{NL}	1	0.222	0.094	5.150	9.312
	7	0.102	0.154	6.080	9.536
	9	0.238	0.151	4.887	8.210
C_L	2	0.301	0.326	5.791	9.144
	5	0.244	0.211	5.241	8.454
	9	0.232	0.308	6.463	9.709

C. EXPERIMENTAL VERIFICATION

Next, we present the experimental verification of some of the theoretical results that have been described in the two previous subsections. In the experimental tests, it was used an electric current demand i identical to that employed for the design of the controllers (see Fig. 7). The tests were performed on the real micro-CHP plant by means of the SCADA system programmed in LabView®. All signals were acquired by this system and then processed in Matlab®. In the next figures, all the experimental signals are represented in blue.

Let us start with the controller x_6^L of C_L. This controller produced an oscillating response when simulated using the nonlinear model (see Fig. 11). Fig. 17 shows the dynamic response of the real system controlled by x_6^L. As can be seen, the oscillations present in the simulation also appear in the real system.

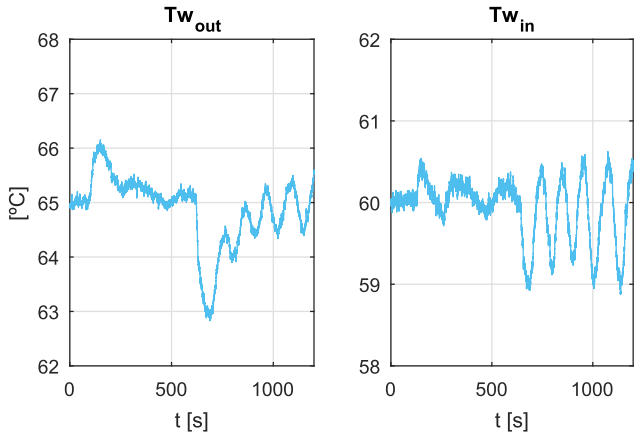

FIGURE 17. Dynamic response of the real system controlled by x_6^L. This controller fails to stabilize the system.

Now let us look at controller $\boldsymbol{x}_{10}^L$, which was the most balanced (lowest value of 2-norm). The performance of this controller suffered a global degradation of 35.19%, the degradation for f_1 being 12.26% (see Fig. 13). Fig. 18 shows the experimental validation of the controller $\boldsymbol{x}_{10}^L$. As can be seen, the experimental response presents a level of degradation similar to that predicted by the theoretical results obtained in simulation.

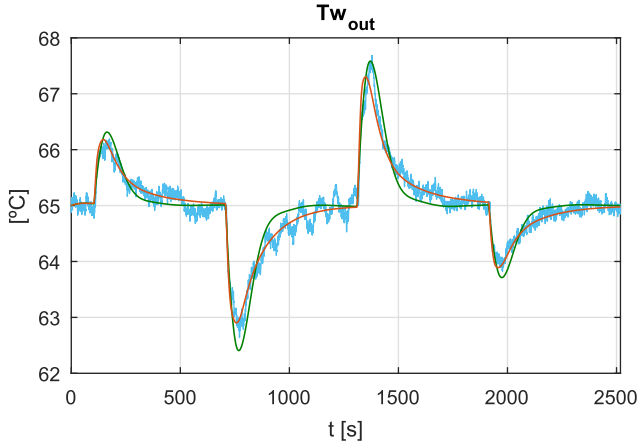

FIGURE 18. Dynamic response of the system controlled by x_{10}^L, in three scenarios: 1) using the linear model (green), 2) using the nonlinear model (red) and 3) using the real plant (blue). The experimental response (blue) corroborates the theoretical response obtained in simulation (red).

It is observed, however, that in the experimental response of the plant controlled by $\boldsymbol{x}_{10}^L$ there appear oscillations which did not exist in the theoretical response. To be more precise, these oscillations are of two different types. The first type (type 1) is the one that is present, especially, in the time intervals 300-600 s and 1500-1900 s, approximately. The second type (type 2) is the one present in the time interval 800-1300 s. They are two distinct types of oscillations because their oscillation frequencies and the causes of their appearance are different.

Type 1 oscillations are due to variations in the hot water tank temperature (T_{t2}). This temperature, which was assumed constant in the design stage, actually shows small variations around 54.45 °C. Fig. 19 shows the signal T_{t2} measured during the test of $\boldsymbol{x}_{10}^L$. This fact has been confirmed. In effect, when the real signal T_{t2} is incorporated into the simulation, then the experimental result coincides, as can be seen in Fig. 20 (noises from the real outputs $T_{w_{out}}$ and $T_{w_{in}}$ are also included in this simulation). The effect of the variations of T_{t2} is not uniform throughout the test. This is because the system is nonlinear. Where they are most noticeable is in the time intervals 100-700 s and 1300-1900 s, i.e. for $i = 200\ A$.

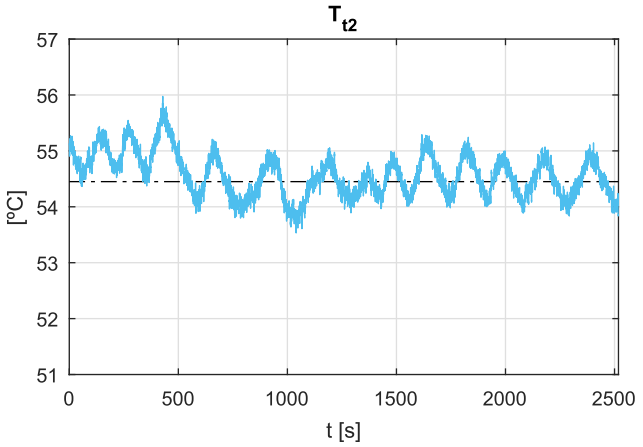

FIGURE 19. Variations in the hot water tank temperature (T_{t2}) during the experimental test of controller x_{10}^L. These variations are the cause of the oscillations (type 1) present in the experimental response of the system controlled by x_{10}^L.

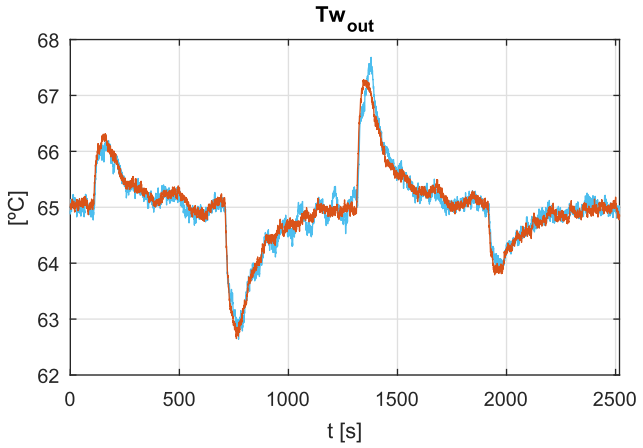

FIGURE 20. When the real signal T_{t2} is incorporated in the simulation, the experimental response of the system controlled by x_{10}^L (blue) coincides with the simulated response using the nonlinear model (red).

In regard to the type 2 oscillations, we believe that they are due to a discrepancy between the nonlinear model and the real plant. In particular, we think that they are due to the fact that in the real plant there is a time delay in the primary cooling circuit which is not perfectly modeled.

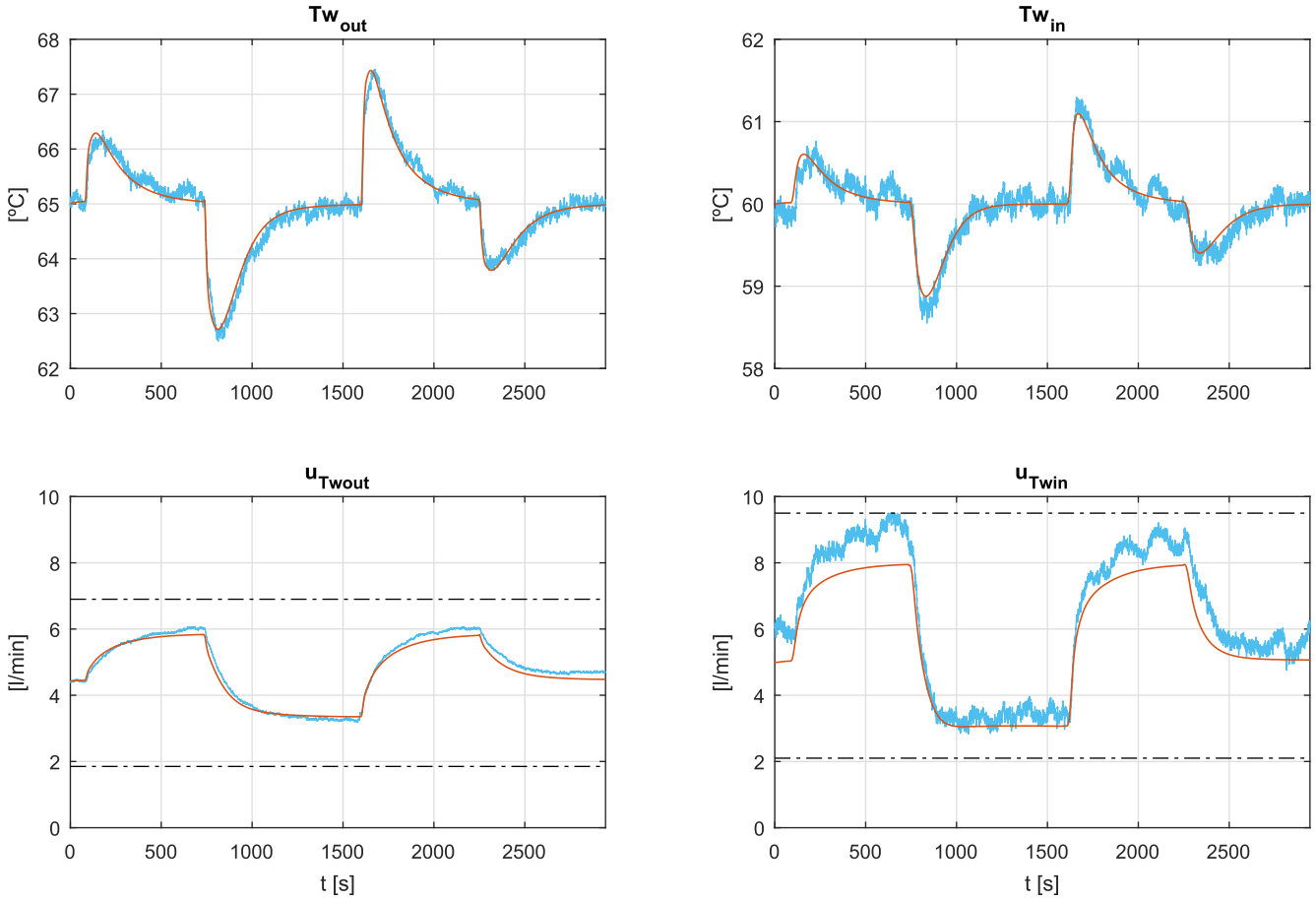

FIGURE 21. Experimental validation of x_1^L, with T_{t2} constant in the simulation and without noises in the outputs (simulation in red, experimental response in blue).

The theoretical results showed that several solutions of C_L did not meet the design requirement regarding the settling time when they were simulated using the nonlinear model (solutions $\boldsymbol{x}_1^L$, $\boldsymbol{x}_4^L$, $\boldsymbol{x}_6^L$, $\boldsymbol{x}_8^L$, $\boldsymbol{x}_9^L$, $\boldsymbol{x}_{10}^L$). Of these, the one that failed to meet it in the greatest degree was $\boldsymbol{x}_1^L$ (see Fig. 14). The experimental validation of $\boldsymbol{x}_1^L$ is shown in Fig. 21 (with T_{t2} constant in the simulation) and in Fig. 22 (with the real signal T_{t2} in the simulation). In both cases, the fit between the experimental response and the simulated response is very satisfactory. In Fig. 23, it can be seen in detail that the controller $\boldsymbol{x}_1^L$, when tested in the real plant, effectively does not meet the requirement of the settling time defined in the design stage, as the theoretical results predicted.

Finally, the theoretical analysis revealed that using the nonlinear model instead of the linear model, solutions with better performance in f_1 can be found. In particular, the best solution of C_L for f_1 ($\boldsymbol{x}_9^L$) and the best solution of C_{NL} for that same objective ($\boldsymbol{x}_{12}^{NL}$) were compared. This comparison displayed an improvement in f_1 of 71.65% (see Fig. 15). When these controllers are tested in the real plant, the experimental results shown in Fig. 24 are obtained. As can be seen, the experimental responses achieved by $\boldsymbol{x}_9^L$ and $\boldsymbol{x}_{12}^{NL}$ corroborate the theoretical results obtained in simulation with considerable accuracy: test signals match simulated ones and the predicted improvement in f_1 is apparent.

VI. DISCUSSION OF RESULTS

We briefly summarize here, before discussion, the main results presented in the previous section:

1) The performance of the controllers designed using the linear model degrades significantly when they are tested on the real plant.
2) In some cases ($\boldsymbol{x}_6^L$) this degradation is such that the dynamic response of the real plant does not stabilize, which is unacceptable.
3) Several of the solutions obtained using the linear model do not meet the design requirements when they are tested on the real system. This is the case of $\boldsymbol{x}_1^L, \boldsymbol{x}_4^L, \boldsymbol{x}_6^L$, $\boldsymbol{x}_8^L, \boldsymbol{x}_9^L$ and $\boldsymbol{x}_{10}^L$, regarding the settling time requirement.
4) The use of the nonlinear model in the control design leads to controllers with better performance in the specified objectives than those obtained using the linear model.

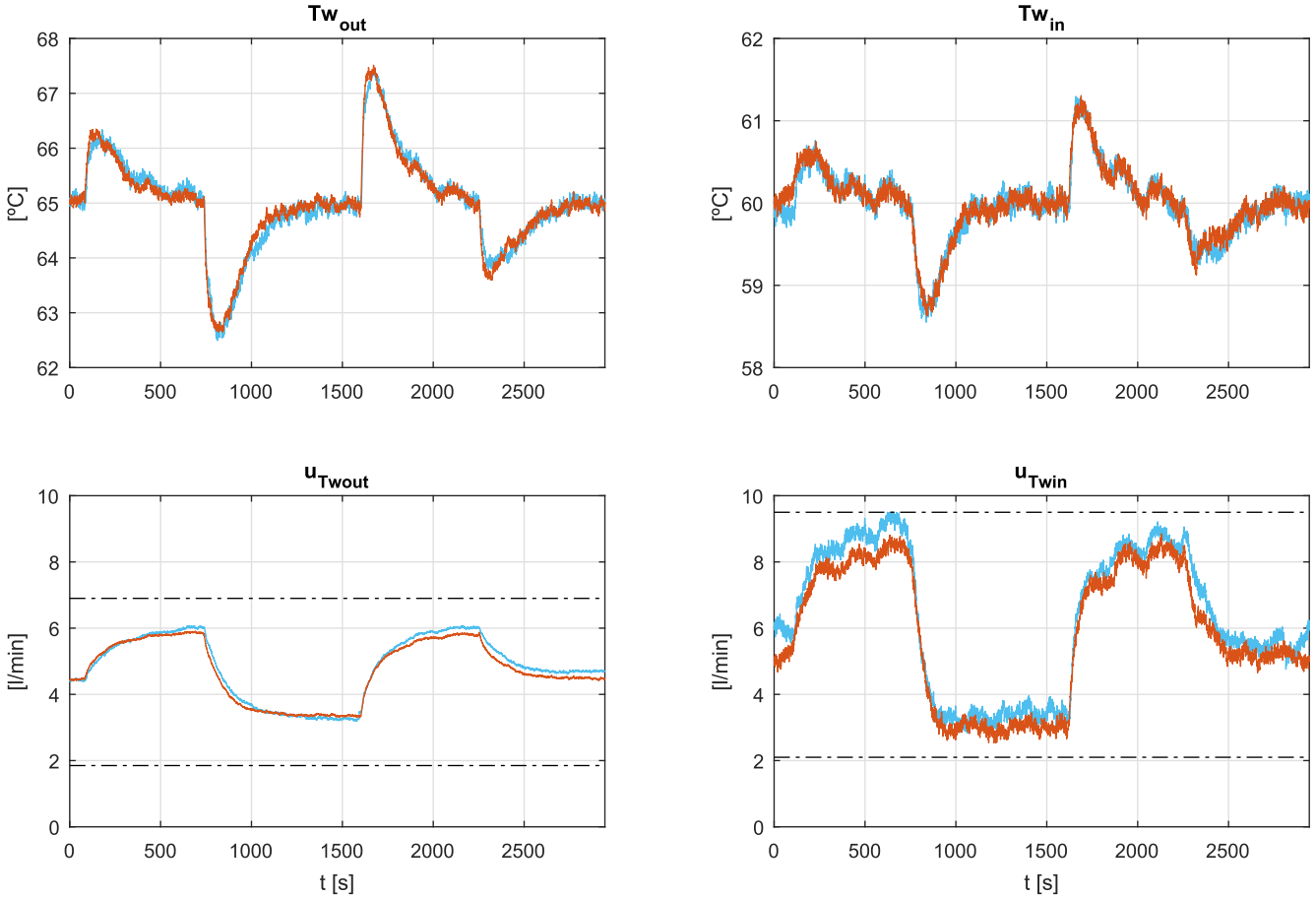

FIGURE 22. Experimental validation of x_1^L. The simulation is carried out including the real signal T_{t2} and the noises in the outputs (simulation in red, experimental response in blue).

5) In particular, if a designer opted to optimize f_1, that is to say, if they chose their controller aiming for the smallest average absolute error in $T_{w_{out}}$, they would find, by using the nonlinear model, a solution ($\boldsymbol{x}_{12}^{NL}$) that is 71.65% better than the best solution that can be found using the linear model for that same objective ($\boldsymbol{x}_9^L$).
6) If a linear model is used for the control design, it turns out that some of the solutions obtained as optimal are not really optimal solutions ($\boldsymbol{x}_2^L$, $\boldsymbol{x}_5^L$, $\boldsymbol{x}_9^L$). The use of a linear model for the temperature control design, therefore, does not guarantee obtaining the optimal solutions (it generates suboptimal solutions). On the other hand, using a nonlinear model, although it does not guarantee it either (because even having a perfect model, there is no certainty that the optimization algorithm converges towards the truly optimal solutions), increases the probability of getting closer to them.

These results demonstrate that using a linear model is inadequate for the design of the temperature control of a PEMFC stack.

In effect, when a linear model is used, the design process ultimately leads to controllers that do not meet the design requirements and that are therefore unacceptable.

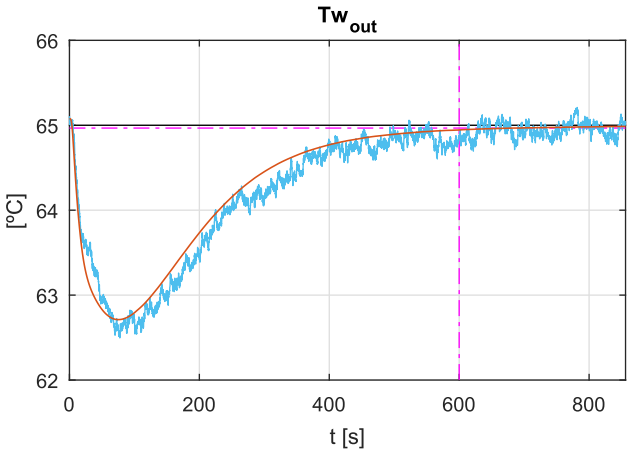

FIGURE 23. Detail of the experimental validation of x_1^L (step at t=700 s). As the theoretical results predicted, the controller x_1^L does not meet the settling time requirement established in the design stage (see equations 19 and 20).

Furthermore, if the controllers are designed using a linear model, the final results that will be achieved in the real plant are unpredictable: the performance of these controllers may worsen or improve with respect to the values calculated in

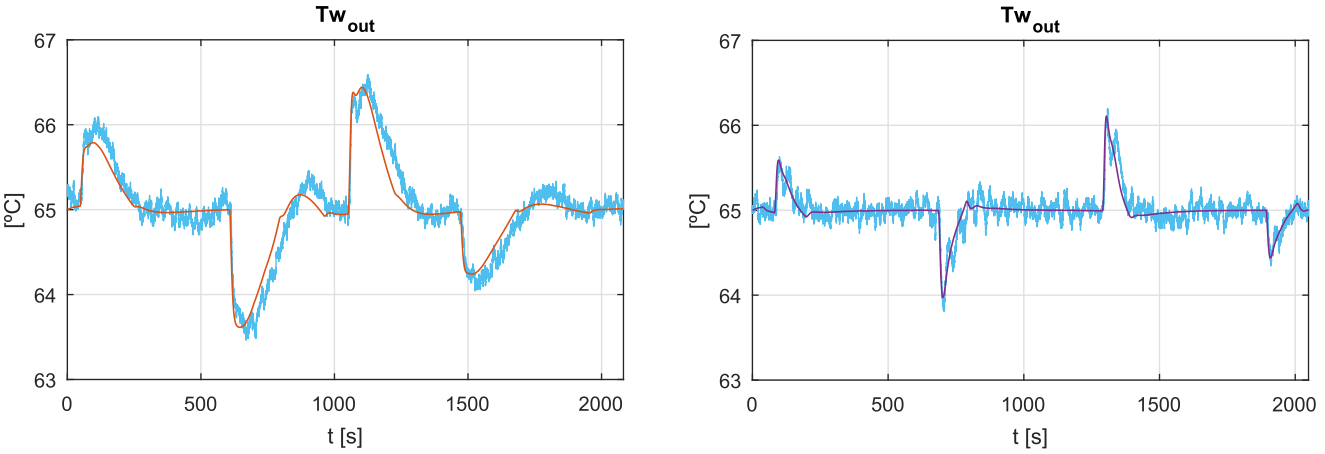

FIGURE 24. Experimental validation of solutions x_9^L (on the left, simulation in red, real response in blue) and x_{12}^{NL} (on the right, simulation in purple, real response in blue). The simulations are carried out with T_{t2} constant and without noises in the outputs.

the design stage. In other words, the true performance that the chosen controller will achieve when tested on the real process can be very different from that foreseen in the design stage, which invalidates the design process itself.

FIGURE 25. PEMFC stack [35].

TABLE 6. PEMFC stack characteristics [35].

Characteristic	Value
Manufacturer	Nedstack
Model	2.0HP
Number of cells	16
Rated power	> 2.0 kWe
Voltage range	9 – 16 V
Current range	0 – 230 A
Weight	14.3 kg
Nominal operating temperature	65 ºC
Heat emission max.	3.3 kW th.
Hydrogen humidity	40% RH
Air humidity	40% RH

The results also show that in order to achieve a superior performance in the temperature control of a PEMFC stack, it is necessary to use a nonlinear model capable of accurately representing the behavior of the real plant within a wide operating range.

Moreover, using a nonlinear model when designing the temperature control is a *sine qua non* condition, since, due to the strong non-linearities of the real system and to the fact that the stack works within a wide operating range, the theoretical results obtained using a linear model valid only around one operating point will not be reproduced in the real plant. In other words, in order the design process itself to be valid, i.e. for its results to be reproducible in the real world, a nonlinear model is necessary.

Finally, the results achieved demonstrate that the use of a nonlinear model allows designers to adequately design the temperature control of a PEMFC stack even using simple control structures, as have been done in this work, where the control structure adopted consists of two PI-type controllers. This is important, because the use of simple (linear) control structures, although it will never provide the optimal performance (since the plant is nonlinear), has some advantages over the use of more sophisticated (nonlinear) control structures, such as simplicity, robustness and computational cost. Therefore, in some cases (for the reasons mentioned) the designer may prefer to maintain a simple control structure. Under this assumption, using our methodology (multiobjective optimization and nonlinear model, see Fig. 5), they will be able to design a controller with better performance, chosen with all the relevant information, and with the guarantee that the controller designed will reproduce its performance in the real plant.

Logically, the use of more sophisticated control structures will result in improved performance. But the use of these more sophisticated control structures only makes sense if a nonlinear model of the real plant, valid within a wide operating range, is available and used for the adjustment of their parameters, since, otherwise, the theoretical results will not be reproduced when the control is tested on the real system. Therefore, the next natural step (a first possible future line of research) is the design of a nonlinear temperature control (sophisticated control) using the same methodology that has been described in this article (see Fig. 5). The performance of this sophisticated control can then be directly compared

to that achieved using a linear control (such as the one presented in this article), thanks to the fact that both controls are optimally adjusted and, consequently, compared under equal conditions, so that the differences in their performance can be specifically attributed to their different structures.

Using a model like the one we have used here for the temperature control design (based on first principles) has still another advantage. As all the model parameters have a real physical meaning, it is possible to analyze the robustness of the designed controllers to uncertainty in the model parameters. This type of analysis (robustness to parameter uncertainties) has been highlighted in the literature as an important aspect in the design of the temperature control of PEMFC stacks [5]. This task could thus constitute a second possible future line of research.

VII. CONCLUSION

Temperature control is crucial to achieve optimal operation in PEMFC stacks, because the performance of this control impacts on the electrical efficiency and lifetime of these devices. Many researchers have pointed out the need to use a nonlinear model in order to design good temperature control. In this article, we have demonstrated that need in an exhaustive and quantitative way. In effect, the performance of half of the controllers designed using the linear model degrades for all design objectives when tested against the nonlinear model (which represents the real plant). In some cases, this degradation is extreme (controller $\boldsymbol{x}_6^L$, average degradation 140.35%), resulting in a dynamic response that never stabilizes (see Fig. 17). Moreover, 6 out of the 10 controllers designed using the linear model fail to meet the design requirements, for example controller $\boldsymbol{x}_1^L$ (see Fig. 14 and Fig. 23).

In the literature, there are many articles on temperature control design for PEMFC stacks, but very few validate their controllers experimentally on a real system. Without an experimental validation, there is no guarantee that the theoretical results are correct. Systems based on PEMFC stacks are complex and, for this reason, in the experimental phase there usually arise pitfalls which were not considered in the theoretical phase. The validity of the theoretical results is always limited and the conclusions drawn from them can only be accepted after their experimental verification. In this work, we have designed a PEMFC stack temperature control based on two PI control loops and the theoretical results obtained in simulation have been experimentally verified. The outcome of this verification is highly satisfactory: the experimental data faithfully reproduce the theoretical results obtained in simulation, as can be seen in figures 17, 18, 20, 21, 22, 23 and 24.

The control design has been carried out using a multiobjective optimization methodology. As far as we know, no one has ever used this methodology before to design the temperature control of a PEMFC stack. This methodology has allowed the consideration of several control objectives simultaneously, which is precisely what must be done, because in the temperature control of a PEMFC stack there is not a single objective, but several. For this reason, this methodology is the most appropriate to solve this control design problem. Any other methodology will always provide partial results (focused on a single objective).

We have also shown that by using a nonlinear model and applying multiobjective optimization, it is possible to arrive at simple temperature control designs (linear control structures) with good performance. This is the case, for example, of controller $\boldsymbol{x}_{12}^{NL}$, which achieves in the stack temperature an overshoot of only 1°C and a settling time of about 100 seconds (see Fig. 15 and Fig. 24). This, in some cases, may be preferred by the designer, due to the advantages that a linear control has over a nonlinear control (simplicity, robustness and computational cost).

Finally, this study suggests two possible future lines of research: 1) design of a sophisticated control using multiobjective optimization and the nonlinear model and 2) analysis of control robustness to uncertainty in the model parameters.

APPENDIX I. EXPERIMENTAL EQUIPMENT

The most important component of the micro-CHP system used to conduct the experimental tests is the PEMFC stack. The stack is shown in Fig. 25 and its basic parameters are listed in Table 6.

The rest of the components of the micro-CHP system are listed below, as well as some of their basic parameters.

- *Air mass flow meter*. Aalborg, model GFC 57, maximun flow rate 200 l/min, maximum pressure drop 690 mbar.
- *Hydrogen mass flow meter*. Aalborg, model GFC 37, maximun flow rate 50 l/min, maximum pressure drop 551 mbar.
- *Air humidifier*. Perma Pure, model FC200-780-7, membrane tubing Nafion®, operating fluid temperature range 1 - 80°C.
- *Hydrogen humidifier*. Perma Pure, model FC125-240-7, membrane tubing Nafion®, operating fluid temperature range 1 - 80°C.
- *Heat exchanger*. Alfa Laval, model AlfaNova 14, fusion-bonded plate heat exchanger, stainless steel, number of channels 9.
- *Electronic load*. Elektro-Automatik, model EL9080-200 HP, input current 0 - 200 A, input voltage 0 - 80 V, input power 0 - 2400 W.
- *Radiator*. Pilan, model TP-10, thermal power dissipated 3000 W (at 10 l/min and ΔT 30 °C).
- *Motorized valve*. Belimo, model TRC24A-SR, torque 2 Nm, nominal voltage DC 24 V, control modulating DC 0 - 10 V, position feedback DC 2 - 10 V, running time 15 s.
- *Pump 1*. Pan World, model NH30PX, 24 VDC.
- *Pump 2*. Pan World, model MD-55R, 220 VAC.
- *Control unit*. National Instruments, model CompactRIO-9014 Real-Time Controller.
- *Computer*. Dell, Intel(R) Core(TM) i7-6700K CPU @ 4.00GHz, RAM 16.0GB, Windows 10 Pro.

REFERENCES

[1] O. Z. Sharaf and M. F. Orhan, "An overview of fuel cell technology: Fundamentals and applications," *Renew. Sustain. Energy Rev.*, vol. 32, pp. 810–853, Apr. 2014.

[2] F. J. Vivas, A. De las Heras, F. Segura, and J. M. Andújar, "A review of energy management strategies for renewable hybrid energy systems with hydrogen backup," *Renew. Sustain. Energy Rev.*, vol. 82, pp. 126–155, Feb. 2018.

[3] M. Carignano, V. Roda, R. Costa-Castelló, L. Valino, A. Lozaño, and F. Barreras, "Assessment of energy management in a fuel cell/battery hybrid vehicle," *IEEE Access*, vol. 7, pp. 16110–16122, 2019, doi: 10.1109/ACCESS.2018.2889738.

[4] W. R. W. Daud, R. E. Rosli, E. H. Majlan, S. A. A. Hamid, R. Mohamed, and T. Husaini, "PEM fuel cell system control: A review," *Renew. Energy*, vol. 113, pp. 620–638, Dec. 2017.

[5] C. Kunusch, P. Puleston, and M. Mayosky, *Sliding-Mode Control of PEM Fuel Cells*. New York, NY, USA: Springer, 2012.

[6] R. Beith, *Small and Micro Combined Heat and Power (CHP) Systems: Advanced Design, Performance, Materials and Applications*. Cambridge, U.K.: Woodhead Pub. Ltd., 2011.

[7] G. Zhang and S. G. Kandlikar, "A critical review of cooling techniques in proton exchange membrane fuel cell stacks," *Int. J. Hydrogen Energy*, vol. 37, no. 3, pp. 2412–2429, Feb. 2012.

[8] S. G. Kandlikar and Z. Lu, "Thermal management issues in a PEMFC stack—A brief review of current status," *Appl. Thermal Eng.*, vol. 29, no. 7, pp. 1276–1280, May 2009.

[9] J.-W. Ahn and S.-Y. Choe, "Coolant controls of a PEM fuel cell system," *J. Power Sources*, vol. 179, no. 1, pp. 252–264, 2008.

[10] Q. Yan, H. Toghiani, and H. Causey, "Steady state and dynamic performance of proton exchange membrane fuel cells (PEMFCs) under various operating conditions and load changes," *J. Power Sources*, vol. 161, no. 1, pp. 492–502, 2006.

[11] W. Yuan, Y. Tang, M. Pan, Z. Li, and B. Tang, "Model prediction of effects of operating parameters on proton exchange membrane fuel cell performance," *Renew. Energy*, vol. 35, no. 3, pp. 656–666, Mar. 2010.

[12] J. Zhang, "The effects of temperature on PEM fuel cell kinetics and performance," in *PEM Fuel Cell Testing and Diagnosis*. Amsterdam, The Netherlands: Elsevier, 2013, pp. 121–140.

[13] W. Schmittinger and A. Vahidi, "A review of the main parameters influencing long-term performance and durability of PEM fuel cells," *J. Power Sources*, vol. 180, no. 1, pp. 1–14, May 2008.

[14] J. Han, J. Park, and S. Yu, "Control strategy of cooling system for the optimization of parasitic power of automotive fuel cell system," *Int. J. Hydrogen Energy*, vol. 40, no. 39, pp. 13549–13557, Oct. 2015.

[15] Z. Han, L. He, Z. Niu, and Z. Liu, "A review and prospect for temperature control strategy of water-cooled PEMFC," in *Proc. 36th Chin. Control Conf. (CCC)*, Jul. 2017, pp. 9062–9068.

[16] J.-L. Casteleiro-Roca, A. J. Barragán, F. Segura, J. L. Calvo-Rolle, and J. M. Andújar, "Sistema híbrido inteligente para la predicción de la tensión de una pila de combustible basada en hidrógeno," *Revista Iberoamericana Automática Informática Ind.*, vol. 16, no. 4, p. 492, 2019.

[17] S. N. Giménez, J. M. H. Dura, F. X. B. Ferragud, and R. S. Fernández, "Control-oriented modeling of the cooling process of a PEMFC-based μ-CHP system," *IEEE Access*, vol. 7, pp. 95620–95642, 2019.

[18] L. Huang, J. Chen, Z. Liu, and M. Becherif, "Adaptive thermal control for PEMFC systems with guaranteed performance," *Int. J. Hydrogen Energy*, vol. 43, no. 25, pp. 11550–11558, Jun. 2018.

[19] J. D. Rojas, C. Ocampo-Martinez, and C. Kunusch, "Thermal modelling approach and model predictive control of a water-cooled PEM fuel cell system," in *Proc. 39th Annu. Conf. IEEE Ind. Electron. Soc. (IECON)*, Nov. 2013, pp. 3806–3811.

[20] Y. Zhao and E. Pistikopoulos, "Dynamic modelling and parametric control for the polymer electrolyte membrane fuel cell system," *J. Power Sources*, vol. 232, pp. 270–278, Jun. 2013.

[21] A. Pajares, X. Blasco, J. M. Herrero, and G. Reynoso-Meza, "A new point of view in multivariable controller tuning under multiobjective optimization by considering nearly optimal solutions," *IEEE Access*, vol. 7, pp. 66435–66452, 2019.

[22] X. Blasco, J. M. Herrero, J. Sanchis, and M. Martínez, "A new graphical visualization of n-dimensional Pareto front for decision-making in multiobjective optimization," *Inf. Sci.*, vol. 178, no. 20, pp. 3908–3924, Oct. 2008.

[23] X. Blasco, J. M. Herrero, G. Reynoso-Meza, and M. A. M. Iranzo, "Interactive tool for analyzing multiobjective optimization results with level diagrams," in *Proc. Genetic Evol. Comput. Conf. Companion*, Jul. 2017, pp. 1689–1696.

[24] C. A. C. Coello, G. B. Lamont, and D. A. V. Veldhuizen, "Multi-criteria decision making," in *Evolutionary Algorithms for Solving Multi-Objective Problems* (Genetic and Evolutionary Computation). New York, NY, USA: Springer, 2007, pp. 515–545.

[25] M. Martínez-Iranzo, J. M. Herrero, J. Sanchis, X. Blasco, and S. García-Nieto, "Applied Pareto multi-objective optimization by stochastic solvers," *Eng. Appl. Artif. Intell.*, vol. 22, no. 3, pp. 455–465, Apr. 2009.

[26] A. Shirazi, M. Aminyavari, B. Najafi, F. Rinaldi, and M. Razaghi, "Thermal–economic–environmental analysis and multi-objective optimization of an internal-reforming solid oxide fuel cell–gas turbine hybrid system," *Int. J. Hydrogen Energy*, vol. 37, no. 24, pp. 19111–19124, Dec. 2012.

[27] L. Khani, A. S. Mehr, M. Yari, and S. M. S. Mahmoudi, "Multi-objective optimization of an indirectly integrated solid oxide fuel cell-gas turbine cogeneration system," *Int. J. Hydrogen Energy*, vol. 41, no. 46, pp. 21470–21488, Dec. 2016.

[28] A. Behzadi Forough and R. Roshandel, "Design and operation optimization of an internal reforming solid oxide fuel cell integrated system based on multi objective approach," *Appl. Thermal Eng.*, vol. 114, pp. 561–572, Mar. 2017.

[29] A. Baghernejad, M. Yaghoubi, and K. Jafarpur, "Optimum power performance of a new integrated SOFC-trigeneration system by multi-objective exergoeconomic optimization," *Int. J. Electr. Power Energy Syst.*, vol. 73, pp. 899–912, Dec. 2015.

[30] S. Sanaye and A. Katebi, "4E analysis and multi objective optimization of a micro gas turbine and solid oxide fuel cell hybrid combined heat and power system," *J. Power Sources*, vol. 247, pp. 294–306, Feb. 2014.

[31] H. Cao and X. Li, "Thermal management-oriented multivariable robust control of a kW-scale solid oxide fuel cell stand-alone system," *IEEE Trans. Energy Convers.*, vol. 31, no. 2, pp. 596–605, Jun. 2016.

[32] H.-B. Huo, Y.-X. Wu, Y.-Q. Liu, S.-H. Gan, and X.-H. Kuang, "Control-oriented nonlinear modeling and temperature control for solid oxide fuel cell," *J. Fuel Cell Sci. Technol.*, vol. 7, no. 4, Aug. 2010.

[33] M. Fardadi, F. Mueller, and F. Jabbari, "Feedback control of solid oxide fuel cell spatial temperature variation," *J. Power Sources*, vol. 195, no. 13, pp. 4222–4233, Jul. 2010.

[34] Y. Qin, G. Zhao, Q. Hua, L. Sun, and S. Nag, "Multiobjective genetic algorithm-based optimization of PID controller parameters for fuel cell voltage and fuel utilization," *Sustainability*, vol. 11, no. 12, p. 3290, Jun. 2019.

[35] *Nedstack PEM Fuel Cell Stack. Intallation and Operation Manual. Rev 1.3 [EN]*, Nedstack Fuel Cell Technol. BV, Arnhem, The Netherlands, Oct. 2013.

[36] W. A. N. W. Mohamed, S. F. A. Talib, I. A. Zakaria, A. M. I. Mamat, and W. R. W. Daud, "Effect of dynamic load on the temperature profiles and cooling response time of a proton exchange membrane fuel cell," *J. Energy Inst.*, vol. 91, no. 3, pp. 349–357, Jun. 2018.

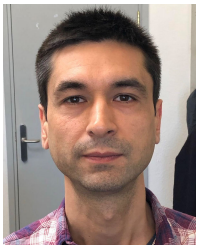

SANTIAGO NAVARRO GIMÉNEZ was born in Valencia, Spain, in 1979. He received the B.S. degree in control systems engineering from the Universitat Politècnica de València (UPV), Spain, in 2004. After working as a Process Engineer for six years in the automotive industry, he joined the Predictive Control and Heuristic Optimization Group (CPOH), Instituto Universitario de Automática e Informática Industrial, UPV, in 2012, where he has been working, since then, on modeling and control design in several projects related to energy management. His main research interests include modeling, control, and energy management of PEMFC-based systems.

JUAN MANUEL HERRERO DURÁ received the B.S. and Ph.D. degrees in control systems engineering from the Universitat Politècnica de València (UPV), in 1999 and 2006, respectively. He is currently an Associate Professor with the Department of Systems Engineering and Automation, UPV. His main research interests include multivariable predictive control, process optimization, and computational intelligence methods for control engineering.

FRANCESC XAVIER BLASCO FERRAGUD was born in Paris, in 1966. He received the B.S. degree in industrial engineering from the Universitat Politècnica de València (UPV), Spain, in 1991, the Diplome de Spécialisation en Génie Electrique degree from the École Supérieure d'Electricité (SUPELEC), France, in 1992, and the Ph.D. degree in industrial engineering from UPV, in 1999. Since 1994, he has been teaching with the Department of Systems Engineering and Automation, UPV. He is currently a Full Professor. His research work was developed at the Institute of Automatic Control (ai2), UPV. His research interests include model-based predictive control, evolutionary optimization, and multiobjective optimization applied to engineering, dynamic modeling, and process control.

RAÚL SIMARRO FERNÁNDEZ was born in Valencia. He received the Ph.D. degree in industrial engineering from the Universitat Politècnica de València (UPV). He has been teaching topics on process control with the Department of Systems Engineering and Automation, UPV, since 2002. His research interests include distributed computer control algorithms for mobile robotics and simulation based on discrete event control.